Fluctuations and anomalous transport in tokamaks

Cite as: Physics of Fluids B: Plasma Physics **2**, 2879 (1990); https://doi.org/10.1063/1.859358
Submitted: 29 September 1989 . Accepted: 28 August 1990 . Published Online: 01 September 1998

A. J. Wootton, B. A. Carreras, H. Matsumoto, K. McGuire, W. A. Peebles, Ch. P. Ritz, P. W. Terry, and S. J. Zweben

Fluctuations and anomalous transport in tokamaks

A. J. Wootton
The University of Texas at Austin, Austin, Texas 78712

B. A. Carreras
Oak Ridge National Laboratory, Oak Ridge, Tennessee 37831

H. Matsumoto
General Atomics, San Diego, California 92133

K. McGuire
Plasma Physics Laboratory, Princeton, New Jersey 08543

W. A. Peebles
The University of California at Los Angeles, Los Angeles, California 90024

Ch. P. Ritz
The University of Texas at Austin, Austin, Texas 78712

P. W. Terry
The University of Wisconsin at Madison, Madison, Wisconsin 53706

S. J. Zweben
Plasma Physics Laboratory, Princeton, New Jersey 08543

(Received 29 September 1989; accepted 28 August 1990)

This is a review of what is known about fluctuations and anomalous transport processes in tokamaks. It mostly considers experimental results obtained after, and not included in, the reviews of Liewer [Nucl. Fusion **25**, 543 (1985)], Robinson [in *Turbulence and Anomalous Transport in Magnetized Plasmas* (Ecole Polytechnique, Palaiseau, France, 1986), p. 21], and Surko [in *Turbulence and Anomalous Transport in Magnetized Plasmas* (Ecole Polytechnique, Palaiseau, France, 1986), p. 93]. Therefore much of the pioneering work in the field is not covered. Emphasis is placed on results where comparisons between fluctuations and transport properties have been attempted, particularly from the tokamak TEXT [Nucl. Technol./Fusion **1**, 479 (1981)]. A brief comparison of experimentally measured total fluxes with the predictions of neoclassical theory demonstrates that transport is often anomalous; fluctuations are thought to be the cause. The measurements necessary to determine any such fluctuation-driven fluxes are described. The diagnostics used to measure these quantities, together with some of the statistical techniques employed to analyze the data, are outlined. In the plasma edge detailed measurements of the quantities required to directly determine the fluctuation-driven fluxes are available. The total and fluctuation-driven fluxes are compared: the result emphasizes the importance of edge turbulence. No model adequately describes all the measured properties. In the confinement region experimental observations are presently restricted to measurements of density and potential fluctuations and their correlations. Various distinct turbulence features that have been observed are described, and their characteristics compared with the predictions of various models. Correlations observed between these fluctuations and plasma transport properties are summarized. A separate section on magnetic fluctuations shows there is very little information available inside the plasma, generally prohibiting quantified comparisons between fluctuation levels and transport. Both coherent and turbulent magnetic fluctuations are addressed, and the differences between low and high plasma pressure (low and high beta) are noted. The contributions of alternate confinement devices, such as stellarators and reversed field pinches, to understanding tokamak anomalous transport are discussed. Finally, future directions are proposed.

I. INTRODUCTION

A. The total fluxes

Transport processes in tokamaks are not generally described by the present neoclassical theories, which account for the effects of Coulomb collisions in toroidal geometry.[1] It is also well known that real plasmas are rarely quiescent; oscillations arise spontaneously.[2–4] In many cases a large number of collective degrees of freedom are excited, defining a state of "turbulence." These fluctuations represent more than harmless oscillations about an equilibrium. We briefly describe how they can affect fluxes of particles and heat, and what measurements are necessary to determine these fluctuation-driven fluxes. Various diagnostics and analysis techniques commonly employed are described, and limitations in both noted.

 0899-8221/90/122879-25$02.00

The main part of the review deals with the measurements of the turbulent fluctuation properties, the implications for fluctuation-driven fluxes, correlations (or otherwise) between fluctuation characteristics and total transport characteristics, and a comparison between the total and fluctuation-driven fluxes. We make extensive use of the reviews already available, by Liewer,[2] Robinson,[3] and Surko.[4] Sections on the plasma edge (defined arbitrarily as $r/a > 0.8$, accessible to material probes in smaller machines) and the plasma interior ($r_{q=1} < r < 0.8a$) are included. Here a is the plasma minor radius and $r_{q=1}$ is the radius, where the safety factor $q = 1$ is taken as the inversion radius of soft x-ray sawteeth.[5,6] In some cases the total fluxes are well described by the measured fluctuation-driven fluxes, i.e., the turbulent fluctuations are responsible for transport. The region $r < r_{q=1}$ is mostly avoided because of sparse data and the complicating sawtooth activity. To provide some consistency, and for simplicity, TEXT[7] results are mainly used for illustrating various points.

Starting with the working particle ambipolar flux Γ^i, it is usually assumed[8] (note superscript i denotes a working ion component) that

$$\Gamma^i = -D^i \nabla n + n v^i, \tag{1}$$

where D^i is the diffusion coefficient, v^i is a convection velocity, and n is the density. By working particle we mean the primary ion species, i.e., H^+, not an impurity such as C. Theoretically, the term nv^i is expected from off-diagonal terms in the transport matrix relating transport fluxes to gradients of plasma parameters.[9] Since both D^i and v^i can depend on fluctuation levels that in turn can depend on density gradients, the flux Γ^i cannot necessarily be partitioned into a diffusive and a convective term. However, the separation is commonly used. Γ^i is determined experimentally from spectroscopic measurements of the particle source S (using H_α light emission) by invoking continuity:

$$\frac{\partial n}{\partial t} = -\nabla \cdot \Gamma^i + S. \tag{2}$$

Behind a limiter, parallel and perpendicular flow[1] can be balanced to derive a radial diffusion coefficient $D^i \approx 1\ \mathrm{m^2\ sec^{-1}}$. In the plasma interior the coefficients D^i and v^i are separately determined by following the time response of the density profile to a perturbation, e.g., an oscillating gas feed,[10] density sawteeth,[11] or a pellet of solid fuel.[12] The results again show $D^i \approx 1\ \mathrm{m^2\ sec^{-1}}$, while $v^i \approx 10\ \mathrm{m\ sec^{-1}}$; both of these values are larger than the neoclassical values[13,14] $D^{i,\mathrm{nc}} \approx 1 \times 10^{-3}\ \mathrm{m^2\ sec^{-1}}$ and $v^{i,\mathrm{nc}} \approx 1\ \mathrm{m\ sec^{-1}}$. The experimental values are described as being anomalous (i.e., anomalously large). However, there are some reported cases, near the plasma axis, where v^{nc} is in agreement with the experimental values.[15–17]

Impurity particle fluxes are determined, like the working gas fluxes, from following time-dependent perturbations.[18] The results are also conventionally described by a diffusion coefficient D^z and a convection velocity v^z. Typical results show $D^z \approx D^i \approx 1\ \mathrm{m^2\ sec^{-1}} \approx 10 D^{z,\mathrm{nc}}$, with $D^{z,\mathrm{nc}}$ the neoclassical value.[18,19] The scalings of D^z and D^i with global plasma parameters are not the same. The technique used results in an intrinsic spatial weighting of v^z toward the plasma edge, and of D^z toward the plasma center. The inward convection velocity $v^z \approx v^{z,\mathrm{nc}} \approx 10\ \mathrm{m\ sec^{-1}}$. Certain characteristic features of impurity behavior *are* predicted by neoclassical theory,[18,20] e.g., impurity accumulation with coneutral beam injection or pellet injection without sawteeth, and impurity expulsion with counter neutral beam injection or suitably chosen asymmetric working gas feed.

Momentum diffusivity is determined by following the response of the plasma rotation velocity to a momentum source. The results are generally interpreted in terms of an anomalous viscosity (see, e.g., Ref. 21), although a neoclassical gyroviscous model has been proposed to explain the results.[22] This mechanism does not explain rotation results from TFTR.[23]

Thermal fluxes (q) and diffusivities (χ) are determined from an analysis of the radial profiles of input power, electron temperature T_e, ion temperature T_i, density n, radiation P_{rad}, charge exchange loss P_{cx}, and particle source S. The electron heat flux deduced (as a remainder) is always anomalously high, being typically 10^2 to 10^3 times the neoclassical prediction.[1] Propagation of locally produced heat pulses gives a value a few times that derived from the profile analysis.[24,25] Ion thermal fluxes are closer to the neoclassical predictions, but as more detailed information on $T_i(r)$ has become available, ion thermal diffusivities $\chi_i > 10\chi_i^{\mathrm{nc}}$ have been found,[21,26] with $\chi_i \approx \chi_e \approx 4D^i$ (although recent JET[27] results show $\chi_e \approx 7D^i$).

B. The fluctuation-driven fluxes

Neoclassical predictions assume that the density n, electric field E, temperature T, magnetic field b, and current density j are stationary. Let the respective fluctuating quantities be represented by $\tilde{n}$, $\tilde{E}$, $\tilde{T}$, $\tilde{b}$, and $\tilde{j}$, respectively. Ignoring poloidal and toroidal asymmetries,[28] and assuming $\omega \ll \omega_{ci}$ (the ion cyclotron frequency), then the fluctuation-driven radial fluxes (denoted by superscript f) for each species (subscript j) are given by electrostatic (superscript E) and magnetic (superscript b) terms:[9]

$$\text{Particle flux:}\quad \Gamma_j^f = \Gamma_j^{f,E} + \Gamma_j^{f,b}, \tag{3}$$

$$\Gamma_j^{f,E} = \langle \tilde{E}_\theta \tilde{n}_j \rangle / B_\phi, \tag{4}$$

$$\Gamma_j^{f,b} = -\langle \tilde{j}_\parallel \tilde{b}_r \rangle / (eB_\phi) = g_1(\tilde{b}_r/B_\phi); \tag{5}$$

$$\text{Energy flux:}\quad Q_j^f = Q_j^{f,E} + Q_j^{f,b}, \tag{6}$$

$$Q_j^{f,E} = \tfrac{3}{2} k_b n \langle \tilde{E}_\theta \tilde{T}_j \rangle / B_\phi + \tfrac{3}{2} k_b T_j \langle \tilde{E}_\theta \tilde{n}_j \rangle / B_\phi, \tag{7}$$

$$Q_j^{f,b} = g_{2j}(\tilde{b}_r/B_\phi) \nabla T_j. \tag{8}$$

These equations represent the effects of electrostatic drifts and of transport in stochastic magnetic fields. Here, k_b is Boltzmann's constant, subscripts, $r, \theta, \phi, \parallel, \perp$ refer to radial, poloidal, toroidal, parallel, and perpendicular to the magnetic field, and $\langle \cdots \rangle$ denotes an ensemble average (we have assumed a circular cross section). The exact form for the functions $g_1(\tilde{b}_r/B_\phi)$ and $g_2(\tilde{b}_r/B_\phi)$ depends on the exact plasma parameters,[2] but typically $g_1(\tilde{b}_r/B_\phi)$ is negligible in tokamaks and g_2 for electrons is taken as the quasilinear expression:

$$g_{2e}(\tilde{b}_r/B_\phi) \approx \pi R v_{the} (\tilde{b}_r/B_\phi)^2 \quad \text{(collisionless plasma)}, \tag{9a}$$

$$g_{2e}(\tilde{b}_r/B_\phi) \approx \chi_{e\|} (\tilde{b}_r/B_\phi)^2 \quad \text{(collisional plasma)}, \tag{9b}$$

with v_{the} the electron thermal velocity, $\chi_{e\|}$ the classical parallel electron thermal diffusivity, and R the plasma major radius. However, in strong turbulence (superscript ST) regimes the collisionless expression for electrons is modified to[2]

$$g_{2e}^{ST}(\tilde{b}_r/B_\phi) \approx \delta_\perp v_{the} [(\tilde{b}_r/B_\phi)^2]^{1/2} \quad \text{(collisionless plasma)}, \tag{10}$$

with $\delta_\perp = k_\perp^{-1}$, a perpendicular wavelength.

It is customary to split the energy flux Q into a conducted heat flux q and the convected flux $\frac{5}{2}k_b T_j \Gamma_j$:

$$Q_j = q_j + \tfrac{5}{2} k_b T_j \Gamma_j, \tag{11}$$

so that

$$q_j = \tfrac{3}{2} k_b n \langle \tilde{E}_\theta \tilde{T}_j \rangle / B_\phi + g_{2j}(\tilde{b}_r/B_\phi) \nabla T_j - k_b T_j \Gamma_j. \tag{12}$$

There is a disagreement in the literature as to whether the factor in the electrostatic component of the energy flux [Eq. (7)] is $\frac{3}{2}$ or $\frac{5}{2}$: the difference is related to the contribution made to the energy source by the turbulence,[9] $\langle \tilde{E} \tilde{j} \rangle$. Theoretical models usually provide Q, independent of the choice of constants. Results from TFTR[29] suggest that the convected energy flux is $\frac{3}{2}k_b T_j \Gamma_j$, rather than $\frac{5}{2}k_b T_j \Gamma_j$, i.e., a factor $\frac{3}{2}$ should be used in Eq. (11).

C. Diagnostics for measuring fluctuations

If $\tilde{n}$, $\tilde{E}$, $\tilde{T}$, and their correlations could be measured throughout the plasma volume, the electrostatic components of the various fluctuation-driven fluxes could be determined identically. This is possible at the plasma edge using probes. For example, the electrostatic particle flux $\Gamma^{f,E}$ is measured as a function of frequency $\omega/(2\pi)$ over a spectral width $d\omega$ in terms of the root-mean-square (rms) fluctuation levels due to the spectral components of width $d\omega$ centered at ω and is given by[30]

$$\Gamma^{f,E}(\omega) = \tilde{n}_{rms}(\omega) \tilde{\phi}_{rms}(\omega) |\gamma_{n\phi}(\omega)| k_\theta(\omega) \times \sin[\alpha_{n\phi}(\omega)]/B_\phi, \tag{13}$$

where k is the measured wave number, $\tilde{\phi} = -\tilde{E}_\theta/k_\theta$ is the measured fluctuating plasma potential, $\gamma_{n\phi}$ is the measured coherence between $\tilde{n}$ and $\tilde{\phi}$, and $\alpha_{n\phi}$ is the measured phase between $\tilde{n}$ and $\tilde{\phi}$. To determine the electrostatic energy flux $Q^{f,E}$ we need the correlation between $\tilde{E}$ (or $\tilde{\phi}$) and $\tilde{T}$, which is not generally known. However, an upper bound can always be placed by assuming perfect correlation [i.e., $\gamma_{T\phi} = 1$, $\sin(\alpha_{T\phi}) = 1$]. To estimate the magnetic components $\Gamma^{f,b}$ and $Q^{f,b}$ we should measure $\tilde{j}_\|$ and $\tilde{q}_\|$ (the parallel heat flux), but this is not done. Instead $\tilde{b}$ is measured, and then models are applied [e.g., Eq. (9) or (10)] to derive the fluxes. Note that, in the rest of this paper, we loosely use $\tilde{n}$, $\tilde{b}$, etc., to represent rms values.

In the plasma edge we can measure or estimate all the required terms, derive the turbulence-driven fluxes, and compare them with the total measured fluxes Γ^i and Q^i to determine if the measured fluctuations play an important role in plasma transport processes. However, there is disagreement on which model to use for the magnetic components (i.e., are the fields stochastic, and should the turbulence be treated as quasilinear or strong?), and what should be used for the parallel autocorrelation length.

In the plasma confinement region the diagnostic problem is more difficult, because the high parallel heat flux precludes the use of material probes. Table I summarizes some of the more commonly used diagnostics with typical resolutions; more details are available in Refs. 31, 32, 33, and 34. Table II summarizes some of the statistical techniques employed to analyze the time series and spatial data into something more readily understood, and more easily compared with theory.[30,35,36] Scattering of microwaves or laser light (e.g., see Refs. 31, 32, 33, and 34), together with fast Fourier transform (FFT) spectral analysis, is commonly used to determine the spectral power density distribution function $S(k,\omega)$, where[37]

$$\langle |\tilde{n}|^2 \rangle = (2\pi)^{-4} \int dk^3 \, d\omega \, S(k,\omega). \tag{14}$$

From this measurement we can determine the frequency-integrated spectral density function $S(k) \propto \tilde{n}(k)^2$, the wave number-integrated spectral density function $S(\omega) \propto \tilde{n}(\omega)^2$, and various spectral averages [e.g., $\bar{v}_{ph} = \Sigma_{\omega,k}(\omega/k) S(k,\omega)/\Sigma_{\omega,k} S(k,\omega)$, $\bar{k} = \Sigma_{\omega,k} k S(k,\omega)/\Sigma_{\omega,k} \times S(k,\omega)$] (see, e.g., Refs. 38 and 39). Typically $0 < k_\perp < 15$ cm^{-1} (where $\mathbf{k}_\perp = \mathbf{k}_r + \mathbf{k}_\theta$). With heterodyne detection[40] the electron drift direction and ion drift direction spectral density functions (S_e and S_i) can be separated.[41,42] A significant advantage of wave scattering is that $\mathbf{k}$ is well defined. However, line of sight measurements (subscript los), or measurements with little spatial resolution, are often used.

Another diagnostic, the heavy ion beam probe (HIBP)[43,44] allows simultaneous measurements of both density and potential fluctuations summed over a large range of k, $0 < k_\perp < 50$ cm^{-1}, together with $\alpha_{n\phi}$ and $\gamma_{n\phi}$ for $0 < k_\perp < 5$ cm^{-1}. While the scattering techniques measure the k spectrum directly, both the HIBP and Langmuir probes utilize a two-point correlation technique.[30,45] This adaption of the linear FFT spectral analysis allows fluctuation-driven fluxes to be deduced. However, the technique is limited in the interpretation of average quantities (e.g., $\bar{k}$, $\bar{v}_{ph}$) if two distinct turbulence features coexist. For example, only the total $\tilde{n}/n$ is measured, not $\tilde{n}/n$ from each turbulence feature separately. Thus counterpropagating features such as a coexisting electron and ion feature cannot be separated, and microscopic details of each individual feature cannot be isolated for comparison with theoretical expectations. Further, $\alpha_{n\phi}$ and $\gamma_{n\phi}$ will be affected, and $\Gamma^{f,E}$ from the HIBP may be incorrect. This limitation is proving particularly troublesome when both electron drift and ion drift features are present, and only the characteristics of the electron drift feature are wanted for a detailed comparison with theoretical predictions. Homodyne detection of wave scattering also loses information if such counterpropagating turbulence exists.

TABLE I. Diagnostics used to deduce fluctuation characteristics.

Langmuir probe (74,82,94)	$\tilde{n}$, $\tilde{\phi}$, $\tilde{E}$, $\tilde{T}$, $\mathbf{k}$, v_{ph}, $\alpha_{n\phi}$, α_{ET}, $\Gamma^{f.E}$, $Q^{f.E}$. Restricted to edge plasmas ($T<50$ eV). $1<k<10$ cm^{-1}: could go both smaller and larger. Sensitive to nonthermal energy distributions.
Scattering (31,32,33,34)	$\tilde{n}$, $\mathbf{k}$, v_{ph}. Spatial resolution: mostly line of sight integrated. k resolution (by geometry and λ): $0<k<20$ cm^{-1}, some larger. Heterodyne detection resolves counter propagating turbulence.
HIBP (43)	$\tilde{n}$, $\tilde{\phi}$, $\tilde{E}$, $\mathbf{k}$, v_{ph}, $\alpha_{n\phi}$, $\gamma_{n\phi}$, $\Gamma^{f.E}$, maybe $\tilde{b}$. Spatial resolution: (r, θ, ϕ) 1 cm$\times$5 mm$\times$1 mm. k resolution: $0<k<50$ cm^{-1} for $\tilde{n}$, $\tilde{\phi}$, $0<k<5$ cm^{-1} for $\alpha_{n\phi}$, $\gamma_{n\phi}$. Restricted to $T_e>30$ eV, for $\rho=0$ $\bar{n}_e>3\times10^{19}$ m^{-3}, $B_\phi<2.2$ T. If $\tilde{T}_e\neq0$ then $\tilde{n}/n$ good only for $T_e>100$ eV.
Reflectometry (46,47,48,49)	$\tilde{n}$. Spatial resolution: determined by ∇n, radial $\sim mm$ possible. k resolution: poor.
Soft x ray (31,32,33,34)	$f(n, T,$ impurity): used for coherent modes. Spatial resolution: line integrated.
Hard x ray (55,56,57)	Runaway electron monitor, implies $\tilde{b}$ using theory. Spatial resolution: none in usual technique.
Induction coils (76.172)	$\tilde{b}$, $\mathbf{k}$, v_{ph}. Spatial resolution: <1 cm. k resolution: <3 cm^{-1}: could go higher. Restricted to edge plasma ($T<50$ eV), often used outside plasma. Could use spatial decay to infer internal $\tilde{b}$.
Optical (51)	$f(n, T,$ impurity$)\Rightarrow\tilde{n}$. Spatial resolution: chord averaged, unless local source used.
ECE (52,53)	$\tilde{T}_e$ (not yet performed). Spatial resolution: R: mm, z: 2 to 4 cm. Presently limited by thermal noise to $\tilde{T}_e/T_e\sim0.01$.

Reflectometry[46–50] is now being used to monitor density fluctuations. Although there are some questions concerning the interpretation of the data, this technique provides a comparatively cheap and simple monitor of changing levels of $\tilde{n}$. Note that this technique gives $\tilde{n}$ at a particular value of n, rather than at a particular location in space. Optical techniques[51] can also be used to provide simple diagnostics for $\tilde{n}$.

Unfortunately no diagnostics yet exist that give relevant information on $\tilde{T}$ in the confinement region,[52,53] and except on small, low-temperature machines (e.g., see Ref. 54) the only information on $\tilde{b}$ is inferred from runaway electron confinement properties.[55–57] Therefore, in the interior of large

TABLE II. Analysis techniques (Refs. 30, 35, 36, 45, 61).

Linear	Nonlinear (Polyspectra)
Stationary **(a) FFT spectral analysis ($P(\omega)$)** $\Rightarrow$ *transport $S(k,\omega)$*	**(a) Bispectral analysis** (three-wave interactions) $\Rightarrow$ *energy cascading wave coupling coefficient connections with theory*
(b) Parametric techniques ($P(\omega)$) e.g., maximum entropy method, or **MEM** short data length, with ω resolution	**(b) Trispectral analysis** (four-wave interactions) $\Rightarrow$ *non-Gaussian nature*
(c) Fractal analysis $\Rightarrow$ *No. of degrees of freedom*	
Nonstationary **(a) short time FFT, MEM ($P(\omega,t)$)**	Nothing developed
(b) Wigner–Ville ($P(\omega,t)$, but sometimes <0)	
(c) Parametric time varying fitting parameters	
(d) Complex demodulation	

Bold: technique, brackets $(\cdots)$: basic information, italics:: detailed information

machines we are restricted to directly measuring only $\Gamma^{f,E}$, with the HIBP. It seems unlikely that we shall be able to measure the correlations necessary to determine identically the internal fluctuation-driven fluxes in the near future (i.e., α_{ET}, γ_{ET}). Therefore, information on $\Gamma^{f,b}$, $q^{f,E}$, and $q^{f,b}$ must come as now from using what we can measure [e.g., $\tilde{n}(k,\omega)$ and $\tilde{\phi}(k,\omega)$] in various models. In the future $\tilde{T}_e$ may become available from electron cyclotron emission (ECE) measurements, and $\tilde{b}$ from HIBP measurements.[58,59]

Having measured interior fluctuating amplitudes, it is natural to seek correlations between this amplitude and plasma transport coefficients. However, one should not necessarily expect to find a direct correlation for three reasons. First comes the problem of possible geometric asymmetries, addressed further in Sec. III B: neither a point nor a line of sight measurement of a fluctuating quantity is adequate. Second comes the choice of applicable turbulence regime [flux $\propto (\tilde{n}/n)^2$, $(\tilde{n}/n)^1$, or $(\tilde{n}/n)^0$ in quasilinear, strong turbulence, and stochastic regimes has been proposed[60]]. However, we should be able to distinguish which is the applicable regime from the measurements of the turbulence microstructure itself. Third, other varying plasma parameters (such as T_e) appear in the relationship between a flux or transport coefficient and a fluctuation level.

As well as improving our arsenal of fluctuation diagnostics, we should improve our statistical analysis techniques. These methods are outlined in Table II. The linear FFT techniques[30,35,45] are well tried, but should be extended to multipoint correlations, perhaps allowing the separation of distinct turbulence features and improving the HIBP capability. Fractal analysis[61] has been applied[62–65] but no deep insight seems to have resulted, except to show that a substantial number of parameters are involved in the processes. Little use is made of the polyspectral techniques,[36] which give information on three- and four-wave coupling, energy cascading, and any non-Gaussian nature of the turbulence. This additional information permits more detailed comparisons between experimental results and theoretical (analytic and numerical) predictions. Conditional sampling techniques likewise have had little application but should be applied, principally to determine the extent to which self-trapping potential structures characterize the turbulence.[66] Also the nonstationary (transient) techniques[36] should be utilized to follow fluctuation responses during and after a perturbation, such as gas puffing,[67] pellet injection,[68] or a sawtooth. Most fluctuation analysis is restricted to steady-state conditions, therefore correlations between fluctuation characteristics and the known and easily recognizable changes in total transport with perturbations are not analyzed. It is often easier to measure correlations between changing parameters during one discharge following a perturbation than to seek correlations between parameters obtained in a series of steady states obtained over many months.

II. THE PLASMA EDGE

A. Turbulence characteristics

We start by presenting some properties of the electrostatic fluctuations, which we will show are largely responsible for edge–particle confinement. The plasma edge is important for two reasons. First, decreasing edge turbulence and (hopefully) increasing edge confinement may insulate the interior plasma, allowing higher internal temperatures. Second, the problem of heat and particle removal to a material surface is partially governed by the perpendicular transport properties. Edge turbulence measurements from diverse machines exhibit a general consistency (see Refs. 2 and 3, and references therein). Figure 1 shows $S(k,\omega)$ obtained on TEXT[69] with a Langmuir probe and FIR scattering, for $\rho = r/a \approx 0.95$. Similar comparisons between probe and scattering results have been made on other machines (e.g., Ref. 70). The results demonstrate the broadband nature of the fluctuations ($\Delta\omega/\bar{\omega} \approx \Delta k_\theta/\bar{k}_\theta \approx 1$) with $\bar{k}_\theta \rho_s \approx 0.05$ to 0.1. Here ρ_s (≈ 0.05 cm) is the gyroradius using T_e and the ion mass m_i, and is a characteristic radial scale length. The fluctuations shown propagate in the electron drift direction, with a phase velocity $\bar{v}_{\rm ph} \approx 3 \times 10^3$ m sec^{-1}. Further out beyond the limiter ($r/a > 1$) $\bar{v}_{\rm ph}$ changes sign. The theoretical expectation[17] $\bar{v}_{\rm ph} = v_{de} - E_r/B$ fits the results well,[39] with $v_{de} = k_b T_e/(eB_\phi L_n)$, where L_n is the density scale length. The frequency broadening demonstrates the turbulent nature, and three-wave interactions play an important role.[36] Other experiments[36,72] show $k_\parallel \approx 10/(qR)$, and a mean $\bar{k}_r = 0$. The anisotropy of the turbulence is expressed by the ratio of the half-widths $\sigma(k)$ of the $S(k_r,k_\theta)$ spectrum (Refs. 39, 60): $\sigma(k_r)/\sigma(k_\theta) \approx 2$, and $\sigma(k_\parallel) \approx k_\parallel$. Only one case of a nonturbulent tokamak edge has been reported,[73] at low I_p and low T_e.

The radial dependence of fluctuating parameters is available from CALTECH,[73–75] MACROTOR,[76–78] TOSCA,[3,79–81] PRETEXT,[82] TEXT,[36,39,69,83–86] TV-1,[87] TJ1,[88,89] DITE,[90] and ASDEX.[91] Figure 2 shows $\tilde{n}/n$, $\tilde{\phi}/(k_b T_e)$, $\tilde{T}_e/T_e$, and $\tilde{b}_r/B_\phi$ for a particular discharge in TEXT as a function of $\rho = r/a$, the flux surface radius normalized to the plasma minor radius. The value $r/a = 1.0$ corresponds to the flux surface just touching the limiter. The results are characteristic of all tokamak edges. Note that

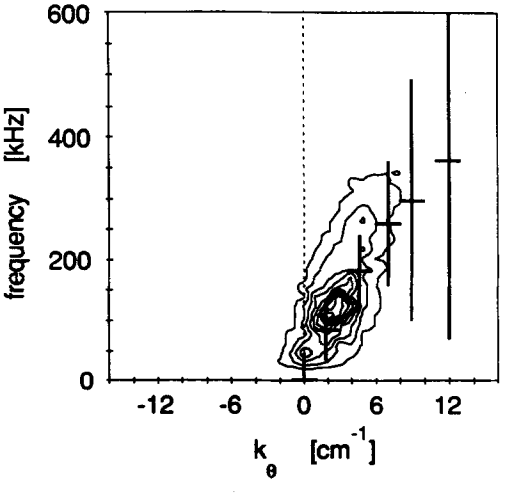

FIG. 1. The $S(k_\theta,\omega)$ spectrum at $r = 0.255$ m in TEXT, from Langmuir probes (contours) and FIR scattering (bars indicate FWHM).

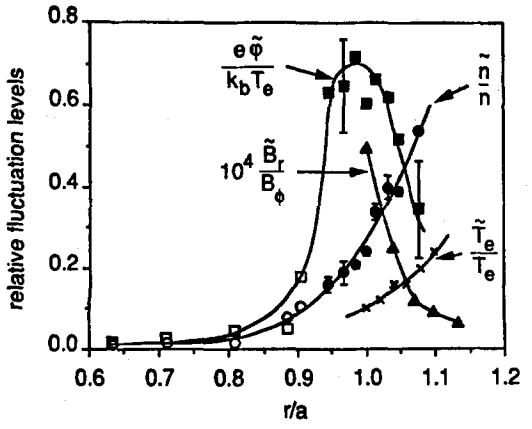

FIG. 2. The spatial profiles near the limiter of $\tilde{n}/n$, $\tilde{\phi}/(k_b T_e)$, $\tilde{T}_e/T_e$, and $\tilde{b}_r/B_\phi$ measured with probes in TEXT ($B_\phi = 2$ T, $I_p = 200$ kA, $\bar{n}_e = 3\times10^{19}$ m^{-3}, H$^+$).

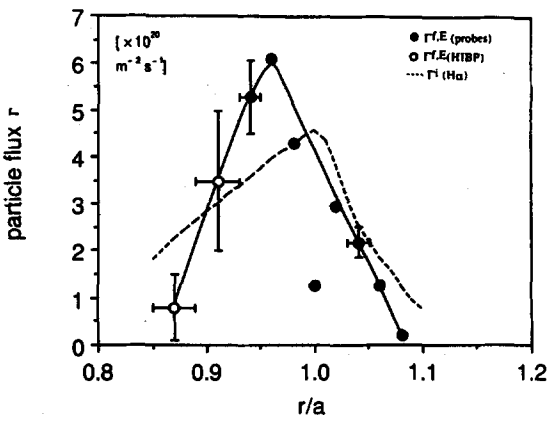

FIG. 3. A comparison of working particle fluxes in TEXT ($B_\phi = 2$ T, $I_p = 200$ kA, $\bar{n}_e = 3\times10^{19}$ m^{-3}, H$^+$), the total Γ^i (from H_α), and $\Gamma^{f,E}$ driven by electrostatic turbulence. $\Gamma^{f,E}$ is measured with Langmuir probes (solid line, solid points) and the HIBP (open points).

$\tilde{\phi}/(k_b T_e) \neq \tilde{n}/n$, and that this departure from the simple Boltzmann relationship is influenced by changing the impurity concentrations.[92] The amplitude of $\tilde{T}_e/T_e$ is still being debated.[75,80,81,86] Poloidal asymmetries in fluctuation levels exist, and are discussed in Sec. III A, with reference to Fig. 5. Discrete limiters are known to affect the steady-state profiles.[93]

Measurements of fluctuating parameters have also been made in reversed field pinches[3,64,94] and stellarators (see Ref. 95 and references therein, and Ref. 96). A comparison shows similar values of $\tilde{n}/n$, $\tilde{\phi}/(k_b T_e)$, and $\bar{k}_\perp \rho_s$ can occur. The power spectra show similar dependencies, $S(k,\omega) \propto \omega^{-p}$ with $p \approx 2$ (although spectral slopes can be only a very weak constraint for testing turbulence theories[97]). Such comparisons should be extended, because they may help isolate the fluctuation driving and damping terms.

B. Particle fluxes

We wish to correlate properties of the electrostatic fluctuations with particle confinement. The electrostatic fluctuation driven flux $\Gamma^{f,E}$ has been measured (determined using Eq. (13), using data similar to that shown in Fig. 1) in Ohmically heated plasmas.[74,75,80,83-85,87,98] A comparison between the total and electrostatic fluctuation driven fluxes has been made,[83] and the scalings and absolute magnitudes of $\Gamma^{f,E}$ and Γ^i at $r = a$, or equivalently the particle confinement times $\tau_p^{f,E}$ and τ_p^i, generally agree. However, asymmetries may affect the agreement. Figure 3 (TEXT) shows an example of the comparison of the radial dependencies of the fluxes near and behind the limiter. A simple model for parallel flow to the limiter[93] at $r/a > 1$, together with Eq. (2), has been used to obtain the perpendicular component Γ^i. The approximate agreement demonstrates that the measured turbulent fluxes account for an important part, if not all, of the total particle fluxes in the edge. The agreement is found for a variety of B_ϕ, I_p, and $\bar{n}_e$. The only case in which $\Gamma^{f,E}$ and Γ^i did not scale together was in the case of improved particle confinement following outward major radial displacements.[83] This has led to suggestions that the particle flux, like the heat flux,[99] is not poloidally symmetric. The observation[85,87] that the peak of $\Gamma^{f,E}$ occurs at $r < a$ may be a result of relative position uncertainties between the probe tips and the calculated last closed flux surface.[84]

Experimental results from the ISX-B tokamak[44] show that neutral beam heating (L mode) reduces τ_p and increases $\Gamma^{f,E}$. The same conclusion (of reducing τ_p and increasing $\Gamma^{f,E}$) is drawn with electron cyclotron resonance heating (ECRH) on DITE.[90] Therefore, the degradation in confinement is associated with an increase in $\Gamma^{f,E}$. No results are available with the H mode,[100] in which improved confinement with additional heating is found, but it seems reasonable to suppose that the improvement in particle confinement is associated with a decrease in $\Gamma^{f,E}$ and mechanisms to explain this should be investigated. Reduced turbulence and increased particle confinement are reported during lower hybrid current drive.[98]

Applying voltages between radially displaced limiters (e.g., limiter and wall) or sandwich limiters has been used to influence electric fields and discontinuities at limiters.[3,80,101-104] An association between negative radial electric field E_r and improved confinement, and positive E_r and degraded confinement, is suggested with neutral beam injection, radio-frequency heating, and biased limiter experiments.[102] Biased limiter results on TEXT show a correlation between reducing E_r (i.e., more negative than the usual value), decreasing Γ^i (improving τ_p and impurity confinement), and decreasing $\Gamma^{f,E}$. Again, the correlation between total and electrostatic fluctuation driven flux is identified. However, no effects on $\Gamma^{f,E}$ from biasing were observed in TOSCA.[3,80] Locally nonambipolar flow[103,105] has been identified behind the limiter ($r > a$).

C. Energy fluxes

The radial variation of the terms in the energy flux Q_e [Eq. (11)] can be deduced,[75,84,85] and the results are shown in Fig. 4 from TEXT. The total fluxes are derived from pro-

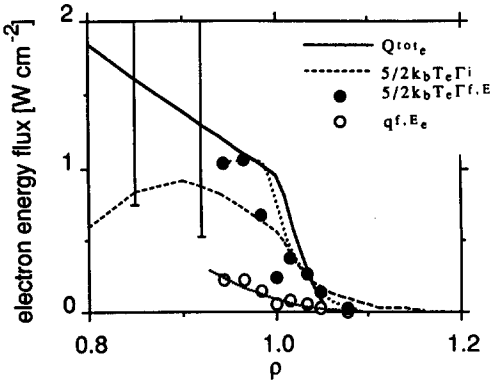

FIG. 4. A comparison of power balance and fluctuation-drive electron energy fluxes in TEXT. Shown are the total (i.e., power balance) conducted and convected electron energy flux Q_e^{tot}, the total convected electron energy flux $5/2k_bT_e\Gamma^i$, the electrostatic fluctuation-driven convected electron energy flux $5/2k_bT_e\Gamma^{f,E}$, and the electrostatic fluctuation-driven conducted electron heat flux $q_e^{f,E}$. The total conducted electron energy flux q_e^{tot} is the difference between Q_e^{tot} and $5/2k_bT_e\Gamma^i$($B_\phi = 2$ T, $I_p = 200$ kA, $\bar{n}_e = 3\times10^{19}$ m^{-3}, H$^+$).

file (power balance) analysis and limiter thermography; the latter confirms the parallel heat flux flowing to the limiter. We find for $\rho > 1$, assuming poloidal and toroidal symmetry, that $>50\%$ of Q_e^{tot} is accounted for by convection ($\frac{5}{2}k_bT_e\Gamma^i$), and that this convected energy flux is explained within the error bars by the measured electrostatic fluctuation driven convected energy flux ($\frac{5}{2}k_bT_e\Gamma^{f,E}$). The total conducted electron energy flux $q_e^{tot} = Q_e^{tot} - \frac{5}{2}k_bT_e\Gamma^i$ is approximately equal to the electrostatic fluctuation-driven conducted energy flux $q_e^{f,E}$ [Eq. (12)]. The measured magnetic fluctuations provide for a very small conducted power loss: $q_e^{f,b} < 1\times10^{-3}Q_e^{tot}$ [Eq. (9)]. Similar conclusions are drawn from results on TOSCA,[106] DITE,[90] and CALTECH.[107] Because of the large uncertainties in the power balance analysis, all of Q_e^{tot} could be explained by convection.[84] At lower densities[85] the edge power balance analysis is more certain (except for the possibility that nonthermal electrons affect the parallel loss term) and shows we cannot account for all of Q_e^{tot} by electrostatic fluctuations. Asymmetries do exist and may play an important role in the analysis. No results are as yet available for either L- or H-mode discharges. Without information on $\tilde{T}_i$ we cannot calculate the fluctuation driven ion thermal fluxes.

D. Theoretical models

Some of the measured fluctuation characteristics are given in Table III, together with the predictions of two models. In one model (drift waves[108]) the turbulence is driven by ∇n, and in another (rippling mode[109,110]) by $\nabla\eta$, the resistivity gradient. Neither model can reproduce all of the observed characteristics. In particular, the ∇n model cannot yet predict the non-Boltzmann like behavior $[\tilde{\phi}/(k_bT_e) \neq \tilde{n}/n]$, the phase angle $\alpha_{n\phi}$, the radial dependence, or the scaling of the fluxes. Experimentally, collisionality seems to be unimportant.[73] The $\nabla\eta$ model fairs better. However, it fails to predict the high poloidal mode numbers ($\bar{m} \approx 50$) which are measured; unless $\bar{m} \approx 5$ is used in the $\nabla\eta$ model, the predicted particle fluxes are too small.[85] Including radiation effects[92] is producing better agreement between experiment and model predictions. Experimentally there appears to be no difference in the turbulence characteristics as the local current density is varied, either by rapidly changing plasma current,[111] or by making comparisons between tokamak and heliotron.[96] This observation has been interpreted as a point against the $\nabla\eta$ model. However, it could be that two different mode types are operative with and without I_p, which happen to have similar characteristics. The Kelvin–Helmholtz instability is also being investigated.[112]

III. THE PLASMA INTERIOR

A. Turbulence characteristics

Less detailed information is available on interior turbulence, although confinement properties are better known than at the edge. The exact parameters required to determine the fluctuation-driven fluxes are not available, and we must interpret the limited data using analytic models. The first part of this section summarizes the characteristics of the turbulence. For simplicity of presentation some edge properties are also included here, although they should properly have been considered in Sec. II. We then discuss particle, electron heat, and finally ion heat, transport.

Figure 5 is a characterization of the results obtained

TABLE III. A comparison between experimentally measured characteristics of the edge turbulence, together with the predictions of two models.

	Exp.	Collisional ∇n models	$\nabla\eta$ models
$\tilde{n}/n$	10%–50%	$\cong\rho_s/L_n$ or $1/k_rL_n \cong 1\%$–20%	$\cong T_e^{-5/6}n^{1/3}B_T^{1/3}q \cong 20\%$
$e\tilde{\phi}/k_bT_e$	$\gtrsim\tilde{n}/n$	$\cong\tilde{n}/n$	$\gtrsim\tilde{n}/n$
$\tilde{T}_e/T_e$	$\cong(0.3\text{–}0.5)(\tilde{n}/n)$	$\tilde{T}_e/T_e \cong 0$	$\cong 0.3(\tilde{n}/n)(L_n/L_{T_e}) \cong (0.2\text{–}0.4)(\tilde{n}/n)$ $\cong 5\%$–15%
$\alpha_{n\phi}$	$0.2\text{–}0.5\pi$	$\cong -\pi$ (stable)	can be large (>0)
$\bar{k}_\theta$	(2–3) cm^{-1}	(2–3) cm^{-1}	$\cong\bar{m}/r \cong 0.5$ cm^{-1}
"m range"	30–100	50–100	<20 for significant power

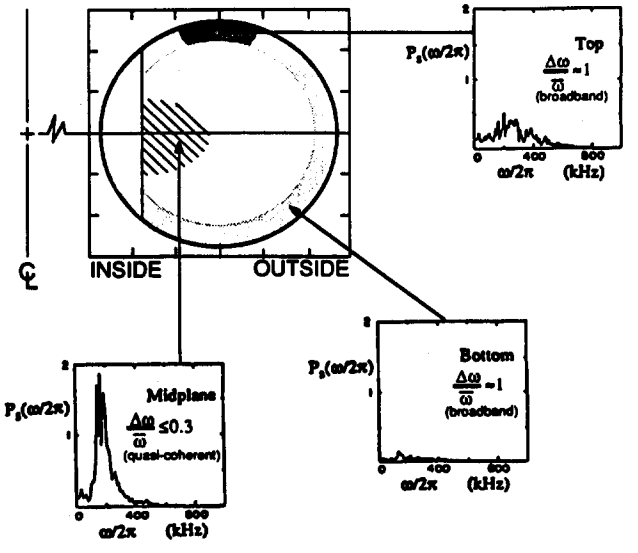

FIG. 5. A sketch of the turbulence from FIR scattering results on TEXT. The density of points is intended to represent the amplitude of $\tilde{n}/n$. Also shown are typical scattered power (P_s) frequency spectra (obtained for $k_\perp = 1\ \mathrm{mm}^{-1}$, with the interaction volume along a vertical chord at $R = 0.95$ m, 5 cm inside of the magnetic axis) above, on, and below the midplane ($B_\phi = 2.8\ \mathrm{T}, I_p = 300\ \mathrm{kA}, \bar{n}_e = 4\times10^{19}\ \mathrm{m}^{-3}, \mathrm{H}^+$). The arrows do not indicate the exact location where the spectra were obtained.

mostly with the scattering diagnostics (see Ref. 2 and references therein, and Ref. 38) in which the density of points is intended to represent the value of $|\tilde{n}/n|$. Also shown are the scattered power (P_s) frequency spectra for $k_\perp = 10\ \mathrm{cm}^{-1}$ at various locations, taken from TEXT.[38] At the plasma periphery the broadband turbulence ($\Delta\omega/\bar{\omega} \geqslant 1$, $\Delta k/\bar{k}_\theta > 1.5$, both FWHM) is found, with $\tilde{n}/n \approx 0.3$. The amplitude generally decreases towards the plasma center where $\tilde{n}/n \approx 0.01$ (exception: ALCATOR-A at reduced parameters, where a peak in $\tilde{n}/n$ at $r/a \approx 0.7$ was found[113,114]), approximately consistent with the mixing length expression[4] $\tilde{n}/n \approx (k_r L_n)^{-1}$. Notable exceptions are TFR,[115-118] where the measured $\tilde{n}/n \approx 0.1\%$, significantly less than the mixing length estimate, and PDX[119] where the scaling was not adhered to. The broadband nature is found independent of sample volume size;[120] this suggests that we are looking at the result of turbulence. In one case (TORTUR[121]) characteristics of growing and decaying modes are found. Most of the power (S) is found at frequencies below 200 kHz, and perpendicular wave numbers $< 1/\rho_s$. However, there is a low-level fluctuation level at all frequencies and wave numbers, whose effects are generally not evaluated. The convenient assumption $\bar{k}_\theta \rho_s \sim$ constant is not found; typically $\bar{k}_\theta \rho_s$ is between 0.05 and 1. The expected B_ϕ dependence is found, but generally no T_e dependence has been identified[4] (exception, ASDEX[122-124]). For example in TEXT[38] $\bar{k} \propto B_\phi^{0.6} I_p^{-0.2}$ and $\bar{k}_\theta \rho_s \approx 0.15$; changing I_p changes T_e. In PDX[119] no difference in the shape of the k spectrum was found between Ohmic and neutral beam heated discharges, although ρ_s changed significantly. Very little, if any, explicit dependence of $\bar{k}$ on ion mass is found (exception, ASDEX[122,124]); the mass scaling of $S(k,\omega)$ needs further investigation. Where measured[2] $\sigma(k_r) \approx \bar{k}_\theta$, and $\bar{k}_\parallel \ll \sigma(k_r), \bar{k}_\theta$. Restricted measurements with an HIBP[125,126] show within large error bars $\tilde{n}/n \approx \phi/(k_b T_e)$, i.e., the Boltzmann relationship may hold in the interior. The fluctuations propagate in the electron diamagnetic drift direction with a typical phase velocity[125] $\bar{v}_{\mathrm{ph}} \approx 5\times10^3$ m sec^{-1}, which may be larger than the expected (Ref. 71) $v_{de} - E_r/B_\phi$.

This broadband turbulence is sometimes up-down asymmetric at the plasma edge[3,127-129]. In ALCATOR[128] an up-down asymmetry preceding MARFES[130] was identified; otherwise it was not present. In TEXT[127] and TOSCA[3,80,129] a different up-down asymmetry was found; in TEXT the asymmetry depends on the direction of the plasma current (the exact scaling of $\tilde{n}/n$ with $\bar{n}_e$ is different at the top and bottom). Such an asymmetry can result from a toroidal asymmetry in the system, e.g., the poloidal ring limiter or the toroidal field ripple, although conflicting evidence exists concerning the role of limiters.[38,77] Up-down asymmetries (as on TEXT and TOSCA) are not generally seen: if present they should have been seen, but were not, on ALCATOR-A,[114] ALCATOR-C,[128] and PDX.[119]

In addition to the broadband turbulence, quasicoherent modes have been found. In TEXT[38,131] a feature with $\Delta\omega/\bar{\omega} \approx 0.1$, $\Delta k/\bar{k}_\theta \approx 0.7$ has been identified at the inner equator, propagating in the electron diamagnetic drift direction with $\bar{v}_{\mathrm{ph}} \approx 1\times10^3$ m sec^{-1}. Although fluctuations with $k_\perp$ rather than k_θ are measured, scans above and below the equator suggest little contribution from radial motion. This velocity is close to v_{de}; one interpretation is that the measured larger $\bar{v}_{\mathrm{ph}}$ for the broadband feature might be a result of modes propagating in the plasma rest frame with velocity $> v_{de}$. Scaling studies of this quasicoherent feature show $\bar{k} \propto B_\phi^{0.7} I_p^{-0.2}$, $\bar{k}_\theta \rho_s \approx 0.6$. The scaling of $\tilde{n}/n$ ($\propto B_\phi^1$) is very different from the broadband feature scaling (where $\tilde{n}/n \propto B_\phi^{-1}$). This feature is not general: it was not found on PLT[132] or PDX.[119] However, a similar quasicoherent mode has been identified on PDX, right at (within 3 to 5 msec) the H-mode onset.[133] In this case the feature had $\omega/(2\pi) \approx 40$ to 100 kHz, $\Delta\omega/\bar{\omega} \approx 0.03$, $m \approx 15$ to 20, and $\tilde{n}/n \approx 1\%$ to 20%. It has been suggested that it may play a role in confinement.

A third feature, broadband and propagating in the ion drift direction, has also been identified.[38,41,42,134] The spectral power density in the ion feature (S_i) relative to that in the broadband electron drift feature (S_e) increases with increasing $\bar{n}_e$. Ignoring complications that arise in the analysis of S_e and S_i from any plasma mass rotation, S_i/S_e increases on TEXT from 0.08 to 0.5 as $\bar{n}_e$ is increased from 2 to 8×10^{19} m^{-3}, with $B_\phi = 2.8$ T and $I_p = 400$ kA. No such feature has yet been found in He discharges, and its strength is reduced when the plasma is fueled with hydrogen pellets, rather than molecular hydrogen and recycled hydrogen ions.[135] An interpretation in terms of the ion temperature gradient mode is discussed in Sec. III D (Fig. 11).

With the above picture it is clear that spatial asymmetries are important, and it is unlikely that any single model will explain all the details of the interior fluctuations. It is also clear that trying to correlate fluctuation levels and confinement properties will be difficult. It is unlikely that we

will ever be able to determine identically the individual fluctuation-driven energy fluxes, as we can at the edge. Instead, we will have to rely on theoretical models to interpret limited data. This is discussed further in Sec. III C. This should not necessarily be regarded as a restriction, because an understanding of the turbulence implies that we have a model to explain it.

Figure 6 shows that radial dependence of $\tilde{n}/n$ for the broadband feature in TEXT as measured with the HIBP diagnostic. Also shown are the predictions of "mixing length" models for drift wave turbulence. These predict that $\tilde{n}/n$ saturates when the convection of perturbed density balances the convection of average density that drives the mode, i.e., when $(\tilde{n}/n) \approx e\tilde{\phi}/(k_b T_e) \approx 1/(k_r L_n)$. For slab geometry[136] $[k_r \approx \rho_s^{-1}(L_n L_s)^{1/2}]$ we have $(\tilde{n}/n)^{\text{slab}} = \rho_s L_n^{-3/2} L_s^{1/2} \approx 3\rho_s/L_n$, while for toroidal geometry[137] $(k_r \approx k_\theta \hat{s})$ we have $(\tilde{n}/n)^{\text{tor}} \approx 1/(k_\theta \hat{s} L_n)$. In these expressions $L_n = -n(dn/dr)^{-1}$, $L_s = Rq/\hat{s}$, and $\hat{s} = (r/q)(\partial q/\partial r)$. It may be reasonable to expect $(\tilde{n}/n) = \min[(\tilde{n}/n)^{\text{slab}}, (\tilde{n}/n)^{\text{tor}}]$. Insufficient information exists at all radii to use measured values of k_θ [which affects $(\tilde{n}/n)^{\text{tor}}$], so the convenient "drift wave scaling" $\bar{k}_\theta \rho_s \approx c$ is invoked, with c being an experimentally determined constant. Both at $\rho \approx 1$ (Langmuir probes, HIBP, FIR) and at $\rho \approx 0.5$ (HIBP) the TEXT results show $c \approx 0.1$. The better representation is then given by $(\tilde{n}/n)^{\text{slab}}$. However, if $c \approx 0.4$, both $(\tilde{n}/n)^{\text{tor}}$ and $(\tilde{n}/n)^{\text{slab}}$ fit the experimental results equally well; values of $c \approx 1$ are found on other machines.[2,4] Neither model predicts the measured $(\tilde{n}/n) \approx 1\%$ at the plasma center.

In this and later comparisons between experiment and theory we would like to use measured characteristics of the electron turbulence feature S_e only. As previously noted the presence of counterpropagating fluctuations in the HIBP data will lead to an underestimate of the relevant value of $\bar{k}_\theta$ and an overestimate of the relevant value of $\tilde{n}/n$. Counterpropagating fluctuations have been seen (the ion feature[38,41,42,134]), but are measured and expected to have a low fluctuation level at low $\bar{n}_e$ (the reason for analyzing a comparatively low density discharge). Using the measured plasma parameters for the particular discharge predicts no ion feature [because the experimental $\eta_i = d\ln(T_i)/d\ln(n_i) < 1.5$, a nominal critical value for instability onset]. However, the experimental uncertainties allow theoretical values[138-140] of $(\tilde{n}/n)^{\eta_i} \approx 1\%$.

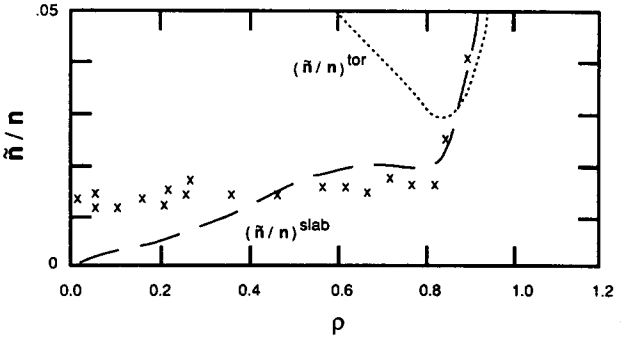

FIG. 6. The spatial variation of $\tilde{n}/n$ from TEXT ($B_\phi = 2$ T, $I_p = 200$ kA, $\bar{n}_e = 2$ to 3×10^{19} m^{-3}, H$^+$), shown as crosses (HIBP). Also shown are the predictions of two mixing length estimates, $(\tilde{n}/n)^{\text{tor}}$ and $(\tilde{n}/n)^{\text{slab}}$. Both electron feature $\tilde{n}/n$ and k_θ ($\bar{k}_\theta \rho_s = 0.1$) are interpreted assuming no ion feature is present.

B. Particle fluxes

In this section we discuss the comparison between total particle flux Γ^i, that driven by the measured electrostatic fluctuations $\Gamma^{f,E}$, and that predicted by drift wave turbulence models, Γ^{dw}. Figure 7(a) shows the radial variation of the working particle flux Γ^i deduced from H_α measurements,[83] together with the electrostatic fluctuation driven flux $\Gamma^{f,E}$ deduced from the HIBP results,[125,141] in TEXT. There is approximate agreement over the region $\rho > 0.6$: for $\rho < 0.6$ the results show $\Gamma^i \approx \Gamma^{f,E} \approx 0$.

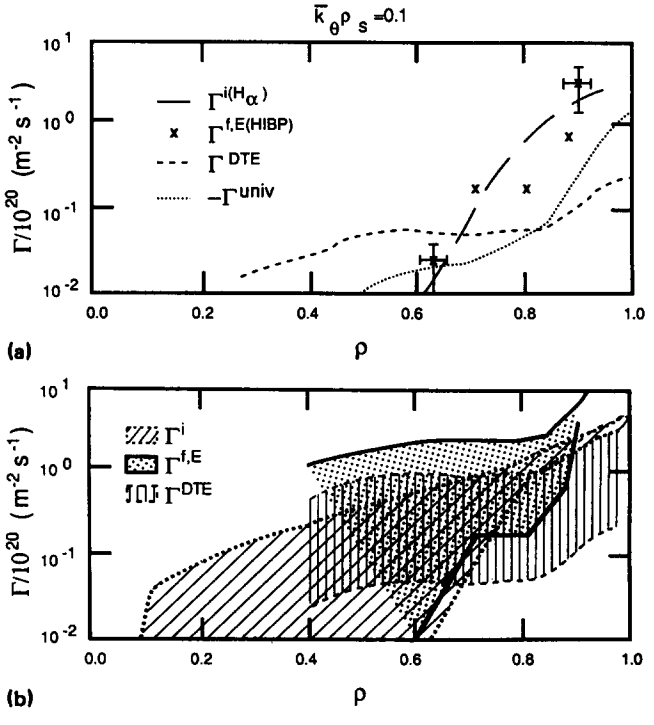

FIG. 7. The spatial variation of working particle fluxes in TEXT ($B_\phi = 2$ T, $I_p = 200$ kA, $\bar{n}_e = 3\times10^{19}$ m^{-3}, H$^+$). Results are shown for the total flux Γ^i, the electrostatic fluctuation driven flux $\Gamma^{f,E}$, and the theoretical expectations from drift wave theory Γ^{DTE} and Γ^{univ}. (a) The total flux $\Gamma^i(H_\alpha)$ deduced from H_α measurements, the electrostatic fluctuation driven flux $\Gamma^{f,E}$ (HIBP) deduced from the HIBP, and two theoretical drift wave estimates, Γ^{DTE} for the (quasilinear, slab) dissipative trapped electron mode and Γ^{univ} for the (quasilinear, slab) universal mode. Both drift wave estimates use measured values of $\tilde{n}/n$ and k_θ ($\bar{k}_\theta \rho_s = 0.1$) interpreted assuming no ion feature is present. Both Γ^{DTE} and Γ^{univ} are shown regardless of the region of applicability. Note that $-\Gamma^{\text{univ}}$ is plotted. (b) Limits to the spatial variations of various working particle fluxes. (1) Γ^ilower $= \Gamma^i(H_\alpha) \approx 0$; (2) Γ^iupper from a neutral particle transport code calculation (ANTIC); (3) $\Gamma^{f,E}$lower $= \Gamma^{f,E}$(HIBP); (4) $\Gamma^{f,E}$upper from $\Gamma^{f,E}$(HIBP) but assuming optimum phase angle and coherence with $\bar{k}_\theta \rho_s = 0.4$; (5) Γ^{DTE}lower using the measured $\tilde{n}/n$ and assuming $\bar{k}_\theta \rho_s = 0.1$; and (6) Γ^{DTE}upper using the measured $\tilde{n}/n$ and assuming $\bar{k}_\theta \rho_s = 0.4$.

The underlying cause of the interior fluctuations has not been identified, but the broadband feature is often assumed to be due to drift waves.[142-144] Also shown in Fig. 7(a) are the fluxes predicted to result from the dissipative trapped electron mode (DTE) and universal mode (univ), both derived in slab geometry from quasilinear flux formulas.[143] Note that the broadband nature ($\Delta\omega/\bar{\omega}\approx 1$) is sometimes invoked to show that quasilinear formulas should not be applied. The dissipative trapped electron mode (DTE) is unstable and the universal mode is stable for the measured k_θ values. However, unstable modes could be excited at higher k and the energy cascade down to the measured k. The expressions for the particle flux are[143,141]

$$\Gamma^{\mathrm{dw}} = n_e (k_b T_e / B_\phi) \Sigma_k [k_\theta (\tilde{n}/n)^2 \delta_e(k)], \tag{15}$$

with the phase angle

$$\alpha_{n\phi} = -\tan[\delta_e(k)], \tag{16}$$

$$\delta_e(k)^{\mathrm{univ}} = [\pi^{1/2}\omega_*/(k_\parallel v_{\mathrm{the}})] \times [k_\perp^2\rho_s^2/(1+k_\perp^2\rho_s^2) - 0.5\eta_e], \tag{17}$$

$$\delta_e(k)^{\mathrm{DTE}} = [4\epsilon^{3/2}\omega_*/(\pi^{1/2}\nu_e)] \times [k_\perp^2\rho_s^2/(1+k_\perp^2\rho_s^2) + 1.5\eta_e]. \tag{18}$$

Here $\epsilon = r/R$, $\eta_e = d\ln(T_e)/d\ln(n_e)$, $k_\parallel \approx 1/(qR)$, ω_* is the diamagnetic frequency, and ν_e is the electron collision frequency. When substituting experimental results in Eq. (15), we perform the indicated summation over k. However, for simplicity of presentation, we discuss the value $\bar{k}_\theta$. In deriving Γ^{dw} we use the HIBP measurements of $\tilde{n}/n(k)$, ignoring complications in data interpretation from the presence of any ion feature. Both Γ^{DTE} and Γ^{univ} are shown regardless of their regimes of applicability; for the discharge considered Γ^{DTE} is applicable for $0.2<\rho<0.7$ and Γ^{univ} is applicable for $0.7<\rho<0.95$. Γ^{DTE} is outward (>0), and Γ^{univ} is inward (<0).

From Fig. 7(a) we would conclude that the total flux is explained by the measured electrostatic fluctuations (although note the role of the neoclassical inward pinch term, discussed below), that the DTE mode does not predict the correct spatial dependence, and that the universal mode predicts an inward instead of an outward flux. However, various limitations on each of the fluxes Γ^i, $\Gamma^{f,E}$, and Γ^{DTE} must be considered, and these limiting fluxes are shown in Fig. 7(b).

First, we consider Γ^i. There is a limitation on the H_α measurement technique because of the inversion procedure necessary to convert from line of sight H_α measurement to a local source. The uncertainties in $\Gamma^i(H_\alpha)$ are very large for $\rho<0.9$: we use $\Gamma^i(H_\alpha)\approx 0$ as a lower limit. If instead of using the "measured" source we use a computed source from a neutral transport code ANTIC,[145] normalized to give the measured particle confinement time, we get a much higher value of Γ^i, and this is used as an upper limit.

Second, the limitations of the HIBP diagnostic in the presence of counterpropagating turbulence must be remembered. In particular, any ion feature (turbulence propagating in the ion drift direction) will reduce $\bar{k}_\theta$, and perhaps distort the phase angle $\alpha_{n\phi}$. Therefore, the flux $\Gamma^{f,E}$ (HIBP) could be incorrect. While the results discussed were obtained in a discharge in which the ion feature was at a very low level (as seen with a wave scattering diagnostic) it is still possible that such an ion feature is affecting the HIBP data, so that $\Gamma^{f,E}$ (HIBP) represents a lower limit to $\Gamma^{f,E}$. To place an upper limit on $\Gamma^{f,E}$ we use the HIBP measured $\tilde{n}/n$, but assume $\alpha_{n\phi}=90°$, $\gamma=1$, and a large value of $\bar{k}_\theta$ (we use $\bar{k}_\theta\rho_s=0.4$).

Third, the value of Γ^{dw} is affected by the choice of $\tilde{n}(k)$, and thus by $\bar{k}_\theta\rho_s$. When using measured values of $\tilde{n}(k)$ in the theoretical expressions [Eqs. (15) through (18)] we should use $\tilde{n}/n(k)$ pertaining only to an electron feature. If an ion feature is present, the experimental $\tilde{n}/n(k)$ measured with the HIBP no longer represents just that part from the electron feature, as discussed previously. To obtain a lower limit on Γ^{dw} we use the measured value of $\tilde{n}/n(k)$, i.e., the measured $\tilde{n}/n$ and the measured $\bar{k}_\theta\rho_s=0.1$. To obtain an upper limit we use the measued $\tilde{n}/n$ and a value $\bar{k}_\theta\rho_s=0.4$.

With these limitations to the fluxes, Fig. 7(b) shows that it is possible that $\Gamma^i=\Gamma^{f,E}=\Gamma^{\mathrm{DTE}}$; Γ^{univ} is still inward (<0). We must reduce these uncertainties by factors >10 before we can show discrepancies between the various fluxes. This demonstrates the difficulties of trying to test theoretical models to determine their relevance, and indicates a necessary future direction for turbulence studies: reducing uncertainties in the measurements.

Although the previous example [Fig. 7(b)] suggested that the total flux Γ^i might be explained by the DTE-driven flux Γ^{DTE}, there is a problem concerning the experimentally observed inward pinch velocity. Working particle fluxes in the plasma interior are characterized by both a diffusive term (D^i) and an inward convective term (v^i) [see Eq. (1), and Refs. 8 and 10]. An example is shown in Fig. 8 for a TEXT discharge;[141] similar results (but with smaller v^i) are also available for T10[15,146] and TFTR.[147] Figure 8(a) shows $D(\rho)$ and Fig. 8(b) shows $v^i(\rho)$; $v^i>0$ is outward. In steady state, with (assumed) no source, the two terms $-D^i\nabla n$ and nv^i exactly cancel. The results of Fig. 7(a) then show that the electrostatic fluctuations must account for both, or neither, of the two terms $-D^i\nabla n$ and nv^i.

We now make a comparison between the experimental values of D and v, and those expected from the DTE and universal drift wave models. To partition Γ^{dw} into a D^{dw} and a v^{dw} we have ignored any dependence of $\tilde{n}/n$ and k_θ on L_n, and taken D^{dw} to be that part of Γ proportional to ∇n. Values are shown only in their approximate regions of applicability. We use the measured $\tilde{n}/n(k_\theta)$ spectra (i.e., $\bar{k}_\theta\rho_s=0.1$, with the caveats discussed in the previous section regarding the effects of S_i on the k_θ and $\tilde{n}/n$ measurement) as a lower limit. We also show the results obtained by assuming $\bar{k}_\theta\rho_s=0.4$, to simulate the effects of removing possible effects of an ion feature in the HIBP data interpretation. The DTE model predicts an outward convection velocity, with negligible diffusion [because $(\bar{k}_\theta\rho_s)^2 \ll 1$; however, the turbulent $\Delta\omega$ affects this term]. Clearly we still require a (theoretical) inward convection velocity. While the uncertainties in the experimental v^i are large, the neoclassical inward pinch[13] v^{nc}, also shown, is generally too small. The universal mode predicts an inward convection velocity, but

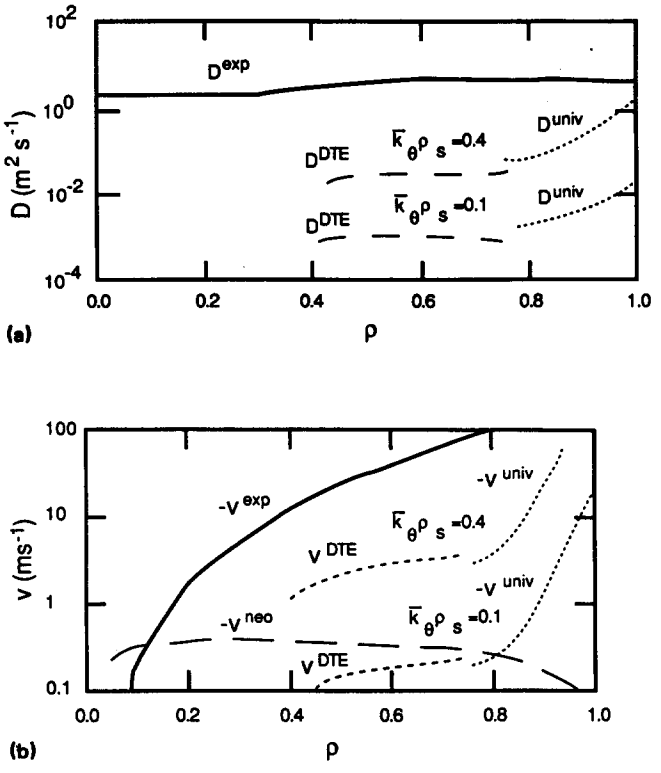

FIG. 8. The spatial variation of working particle diffusion coefficient D (a) and convection velocity v (b) on TEXT ($B_\phi = 2$ T, $I_p = 200$ kA, $\bar{n}_e = 3\times 10^{19}\,\mathrm{m}^{-3}$, H^+). Shown are the experimental values D^{exp} and v^{exp} deduced from oscillating gas puff experiments, together with the predictions of two drift wave turbulence models, dissipative trapped electron (D^{DTE}, v^{DTE}) and universal (D^{univ}, v^{univ}). Both models are for quasilinear turbulence in slab geometry, and evaluated using HIBP measured $\tilde{n}/n$. Results are shown assuming both $\bar{k}_\theta \rho_s = 0.1$ (as measured) and $\bar{k}_\theta \rho_s = 0.4$. Also shown is the neoclassical pinch velocity v^{neo}. Note the signs of v.

is inapplicable in the region $\rho < 0.7$. The ion pressure gradient inward flux[138] is not predicted to be induced in this discharge because $\eta_i < 1.5$, but the uncertainties in η_i are large.

C. Electron energy fluxes

Many experimental groups have sought correlations between fluctuations and (electron) energy transport. While this report concentrates on results from tokamaks, it should be noted that such correlations have been sought in many different magnetic geometries (see, e.g., Refs. 148 and 149). In this section we concentrate on electrostatic fluctuations; Table IV lists some relevant observations deduced mostly from line of sight wave scattering diagnostics. Magnetic fluctuations will be discussed later. As can be seen from the table, extreme points of view are represented. Generally no correlation between $\tilde{n}/n$ and energy confinement time τ_E is found for Ohmic heated discharges; as $\bar{n}_e$ and thus τ_E is increased $\tilde{n}/n_{los}$ remains approximately constant (exceptions, TFR,[150] FT[151]). On TFR[117,118,150,152] a strong correlation between increasing $\tilde{n}/n$ and decreasing electron energy confinement (particularly the conducted component) with additional heating (L mode) was found. On PDX[119] the general correlation between increasing $\tilde{n}/n$ and decreasing confinement was found except for the important case of diverted discharges, Ohmically heated (OH) to L mode. On TEXT[153] and TOSCA[3] little or no increase in $\tilde{n}/n$ was found with ECRH. Both the TFR[117,118] and TEXT[141] groups have claimed that the present quasilinear description of the DTE mode is unsatisfactory in explaining the experimental $\chi_e(r)$ in Ohmic-heated discharges, whereas many predictive code groups claim the quasilinear DTE mode (with additional *ad hoc* assumptions regarding profile consistency) can explain the experimentally observed global transport levels.[154,155]

At this point we should discuss the problems associated with expecting correlations between confinement properties and a fluctuation level. Referring to Fig. 5, it is clear that spatial asymmetries are important, and unlikely that any single model will explain all the details of the interior fluctuations. It is also clear that trying to correlate fluctuation levels and confinement properties will be difficult. It is unlikely that we will ever be able to determine identically the individual fluctuation-driven energy fluxes, as we can at the edge. Instead, we will have to rely on theoretical models to interpret limited data. One should not necessarily expect to find a simple correlation between a line of sight measurement of $\tilde{n}/n$ and a measure of confinement, for example, the heat flux q, the energy confinement time τ_E, or the thermal diffusivity χ_e. This is so for at least three reasons. First, a line of sight (subscript los) value $(\tilde{n}/n)_{los}$ is dominated by edge phenomena, where $\tilde{n}/n$ is largest, and changes in $(\tilde{n}/n)_{los}$ may have nothing to do with changes in internal fluctuation levels. Second, asymmetries change with differing plasma condition, and these can affect $(\tilde{n}/n)_{los}$ even though a local value of $\tilde{n}/n$ has not changed. Third, even if a local measurement of $\tilde{n}/n$ is available, no theory predicts simply that $\chi_e = \text{const} \times (\tilde{n}/n)^a$; other variables appear in the "constant." For example, in quasilinear drift wave theory $a = 2$ and the "constant" $\propto T_e$, among many other parameters. In strong turbulence theories $a = 1$, and it has been suggested that $a = 0$ for stochastic regimes.[60] Notwithstanding these arguments, the results from TFR[150,152] clearly show that $\tau_E^{-1} \propto (\tilde{n}/n)^2$.

To seek correlations between the measured turbulence and q_e^{tot} we should turn to theoretical models. As was done for particle fluxes, we can invoke drift wave models and use the measured values of $\tilde{n}/n(k_\theta)$ in the formulas[143]

$$q_e^{dw} = n_e T_e (k_b T_e / B_\phi) \Sigma_k [k_\theta (\tilde{n}/n)^2 \xi_e(k)], \tag{19}$$

with

$$\xi_e(k)^{univ} = [\pi^{1/2}\omega^*/(2k_\parallel v_{the})] \times [-3k_\perp^2\rho_s^2/(1+k_\perp^2\rho_s^2) + 7\eta_e/2], \tag{20}$$

$$\xi_e(k)^{DTE} = [4\epsilon^{3/2}\omega^*/(\pi^{1/2}\nu_e)] \times [0.5k_\perp^2\rho_s^2/(1+k_\perp^2\rho_s^2) + 15\eta_e/4]. \tag{21}$$

Such calculations were first performed by the TFR team[117,118] for the dissipative trapped electron (DTE) mode. An example of the results from TEXT[141] is given in Fig. 9(a), where the values of q_e^{DTE} and q_e^{univ} are shown in their approximate regions of applicability. Both the DTE and universal (univ) mode predictions show $q_e^{dw} < q_e^{tot}$ in the confinement region. This is in contrast to the results of pre-

TABLE IV. Interior density fluctuations and transport.

Machine	Observation
ASDEX	$\tilde{n}/n_{\rm los}$ constant with increasing $\bar{n}_e$, decreases with increasing B_ϕ.
(68, 122, 123, 124)	k decreases with increasing T_e, or changing from H to D.
	Spectrum broadens in L mode.
	$\tilde{n}$ drops at H-mode transition, inside and outside separatrix.
	Sawteeth affect scattered signals at low $k_\perp$ ($<3\ {\rm cm}^{-1}$).
ATC	$\tilde{n}$ asymmetries found.
(144)	Quasilinear $D\approx\Sigma\gamma_k(k_\theta c_s\rho_s/\omega_k)^2(\tilde{n}_k/n)^2$ would explain χ_e, using measured $\tilde{n}/n$ and estimating $\gamma_k/\omega_k\approx 0.1$
DIII-D	Fluctuations reduced during H mode in (edge) region where L_n decreases.
(50)	
FT	OH: $(\tilde{n}/n)^2_{\rm los}\propto\tau_E^{-1}$ in low $\bar{n}q(a)$, where τ_E is linear with $\bar{n}_e$.
(151)	At higher $\bar{n}q(a)$, where τ_E saturates, the correlation is lost.
	R.F.: little effect on $\tilde{n}$.
JET	Radial correlation length $\sim$2 to 4 cm.
(49)	
JIPTTII-U	Ion feature found when $\eta_i>1$ to 1.2, reduced with pellet injection.
(42)	
PDX	$\tilde{n}/n$ does not scale as mixing length prediction.
(119,133)	Energy in spectrum decreases for $k_\perp\rho_s>0.5$.
	Ballooning nature sometimes observed.
	Limiter plasmas: $\tilde{n}/n\propto(\tau_E)^{-1}$, divertor plasmas: $\tilde{n}/n({\rm OH})\sim\tilde{n}/n$(L mode), although τ_E changes. $\tilde{n}/n$(H mode) $<\tilde{n}/n$(L mode).
	Quasicoherent mode found at H-mode transition.
PLT	Mixing length estimate of $\tilde{n}/n$ satisfied.
(67,120)	$\tilde{n}/n$ increased with increasing inward transport during density rise.
TEXT	Quasilinear $q_e^{\rm dw}$ using measured $\tilde{n}/n$ and k does not fit $q_e^{\rm tot}$.
(40,125,126,127,131,134,135,141,162,164)	Ion feature found, which is reduced with pellet injection.
	Scalings of $\tilde{n}/n$, $\bar{k}$ available.
	An up-down asymmetry and a quasicoherent mode isolated.
	$\tilde{n}/n$ changed $<20\%$ with 200 kW ECRH.
	$\tilde{n}/n$ increases at sawtooth crash.
TEXTOR	Frequency where $\tilde{n}$ is a maximum, and the spectral width in ω, $\propto T_e$.
(159,160,163)	No strong correlation of $\tilde{n}$ at one k with τ_E found (but T_e changing).
	$\bar{n}_e$ scaling: for fixed τ_E, increased $\tilde{n}/n$ corresponds to reduced T_e.
	$(\tilde{n}/n)^2\propto k^{-4}$ for $3\ {\rm cm}^{-1}<k<130\ {\rm cm}^{-1}$.
	$(\tilde{n}/n)$ largest at end of I_p and $\bar{n}_e$ ramp-up phase, corresponding to a T_e dip.
	No systematic effects of ICRF on $\tilde{n}/n$: rather $\tilde{n}^2\propto\lvert L_n\rvert^{-5}$.
	$\tilde{n}/n$ peaks inside limiter radius (at $r<a$).
	$\tilde{n}/n$ increases at sawtooth crash.
TCA	$\tilde{n}/n_{\rm los}$ constant with increasing $\bar{n}_e$, i.e., not correlated with τ_E for OH.
(204)	
TFR	400: $\tilde{n}/n$, k too small to explain χ_e using quasilinear DTE model.
(115,116,117,118,150,152,157,158)	600: $\chi_e^{\rm DTE}(r)$ incorrect using measured $\tilde{n}/n$ and k in quasilinear formula, although absolute value within a factor 4.
	Increasing $\tilde{n}/n_{\rm los}$ correlated with decreasing τ_E with OH, NBI, and ICRF.
	Sawteeth precursors are observed, and a specific turbulence cell is found coincident with the sawtooth crash, within the $q=1$ surface.
TORTUR	$\tilde{n}/n$ studied between 500 Hz to 100 MHz.
(121)	20–700 kHz: structure interpreted as relaxing bursts of drift waves.
	0.7–3 MHz: interpreted as ∇T_e driven turbulence (e.g., microtearing).
	>5 MHz: interpreted as being due to runaway electron interactions.
TOSCA	$\tilde{n}/n$ not changed with ECRH.
(3,70,80,129)	Up-down asymmetry seen.
	$\tilde{n}/n_{\rm los}$ consistent with mixing length, constant with increasing $\bar{n}_e$.

dictive computer codes (see, e.g., Refs. 154, 155, and 156), which claim good agreement with experiment in the DTE regime, i.e., they suggest $q_e^{\rm dw}\approx q_e^{\rm tot}$. The difference between the TEXT experiment and the predictive modeling is primarily that the measured $\bar{k}_\theta\rho_s\approx 0.1$, rather than ≈ 0.5 as is assumed in the codes. However, other tokamaks[2,4] have found larger values of $\bar{k}_\theta\rho_s$, and Fig. 9(b) shows that using $\bar{k}_\theta\rho_s\approx 0.4$ leads to approximate agreement between $q_e^{\rm dw}$ and $q_e^{\rm tot}$ in TEXT [note that in the drift wave values shown in Figs. 9(a) and 9(b) the correct integrals over k are performed]. There is evidence that in TEXT at the lowest densities where data exists (Ref. 153) $\bar{k}_\theta\rho_s\approx 0.35$. This behooves us to better understand the role of the ion feature in the measurements; $S(k,\omega)$, $\bar{k}_\theta$, and $\tilde{n}/n$ include unwanted (for

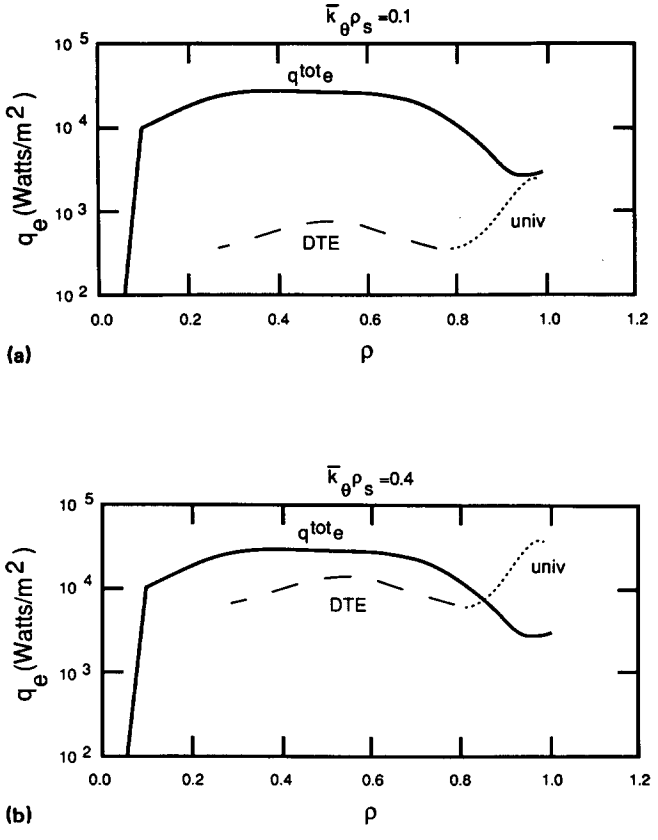

FIG. 9. The radial dependence of the experimental conducted electron heat flux q_e^{tot} in TEXT ($B_\phi = 2$ T, $I_p = 200$ kA, $\bar{n}_e = 3\times10^{19}$ m^{-3}, H$^+$), and the prediction of drift wave turbulence q_e^{dw}. (a) Using experimentally measured turbulence characteristics [HIBP measured $S(k,\omega)$ with both electron feature $\tilde{n}/n$ and k_θ ($\bar{k}_\theta\rho_s = 0.1$) interpreted assuming no ion feature]. Results are shown for the dissipative trapped electron (DTE, broken line) and universal (univ, dotted line) modes. (b) As for (a), but assuming that $\bar{k}_\theta\rho_s = 0.4$, rather than the measured 0.1.

purposes of comparison with drift wave theory) contributions from S_i. However, while accounting for any S_i will increase the relevant $\bar{k}_\theta$, it will decrease the relevant $\tilde{n}/n$ so that the TEXT data may still show $q_e^{dw} < q_e^{tot}$. Further, the discharge analyzed was chosen because the scattering diagnostic showed a very low amplitude ion feature. Other turbulence models should be tested in a similar manner.

Comparison such as those shown in Fig. 9 have not been attempted with additional heating. However, compelling correlations between decreasing confinement time and increasing $\tilde{n}/n$ have been found, and an example from TFR[150,152] is shown in Fig. 10. Figure 10(a) concerns ion cyclotron heating, and Fig. 10(b) concerns neutral beam heating. Small graphic symbols refer to Ohmic heating, and large graphic symbols to additional heating. Here, $\langle\delta n^2/\bar{n}^2\rangle$ is the line of sight frequency-integrated fluctuation level at one k, normalized to the line of sight average density [i.e., $(\tilde{n}_{los}/\bar{n}_e)^2$ in the terminology of this report]. Additionally, τ_T is the electron energy confinement time (conduction and convection) and τ_x the confinement time with the losses from sawteeth removed [see Eqs. (22) and (23)]. Clearly increased electron conduction losses are associated with increased line of sight values of $(\tilde{n}/n)^2$; a similar conclusion is drawn for Ohmically heated discharges. The constant of proportionality between τ^{-1} and $\langle\delta n^2/\bar{n}^2\rangle$ is practically the same for all heating regime studied. The authors emphasize the need for more local measurements.

The observation that χ_e deduced from heat pulse propagation (χ_e^{HP}) sometimes exceeds χ_e from power balance (χ_e^{PB}) might be explained by an increased fluctuation-driven q_e resulting from plasma parameter or gradient changes. Enhancements in $\tilde{n}/n$ coincident with sawtooth collapse are seen on TFR,[157,158] ASDEX,[122] TEXTOR,[159-161] and

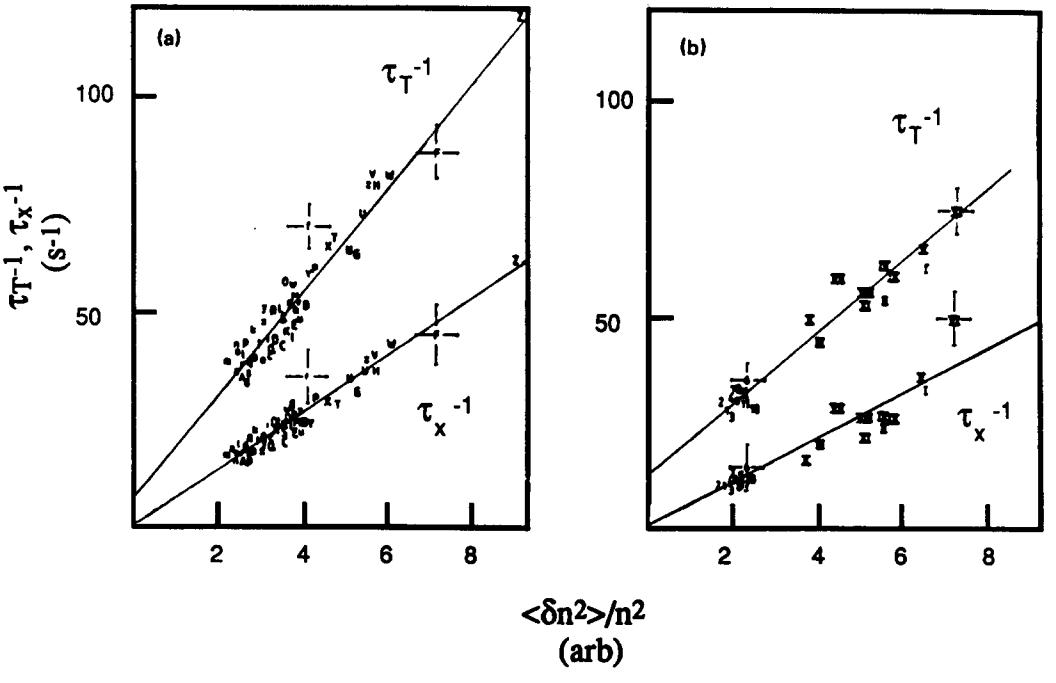

FIG. 10. The correlation between energy confinement time and density fluctuation level obtained on TFR.[150,152] (a) Concerns ion cyclotron heating, and (b) concerns neutral beam heating. Small graphic symbols refer to Ohmic heating, and large graphic symbols to additional heating: $\langle\delta n^2/n^2\rangle$ is the line of sight frequency integrated fluctuation level at one k (6 cm^{-1}), normalized to the line of sight average density $\bar{n}_e$; τ_T is the electron energy confinement time (conduction and convection); and τ_x is the confinement time with the losses from sawteeth removed.

TEXT,[162] but generally with little spatial resolution. In the case of TEXTOR the enhancement is quantitatively reproduced by a heat transport code in which the anomalous electron transport coefficient is calculated self-consistently from a theoretical model for the saturation of the DTE instability. In TFR[158] and TEXTOR[161] a high-frequency (extending at least $3<k<17$ cm^{-1}, $\omega/2\pi\approx 1$ MHz for $k=7$ cm^{-1}) burst is found, at a time corresponding to the collapse and poloidal expansion of the hot core. The cell of enhanced turbulence is localized within $r_{q=1}$, and extends poloidally about 120° to 180°. The heat flux associated with the sawteeth is not poloidally symmetric: the direction of the "sooner and faster" heat flux agrees with the central position of the turbulent cell. Both intrinsic (i.e., plasma-generated[158,163]) and extrinsic (i.e., externally imposed[164]) magnetic islands are found to affect $\tilde{n}/n$ significantly, perhaps demonstrating a sensitivity to local plasma parameters such as L_n.

Alternative models to explain q_e invoke magnetic fluctuations, and measurements to support or disprove this point of view are described in Sec. IV.

D. Ion energy fluxes

Unlike the electron heat flux, the ion heat flux has been thought to be close to the expected neoclassical value.[1] However, as better ion temperature profiles have become available, anomalies (i.e., values inconsistent with neoclassical theory[165]) outside the experimental error bars are being found.[26] As the density is increased by gas puffing in Ohmic-heated discharges a saturation in global energy confinement time τ_E is found[1]. Figure 11 shows an example from ALCATOR-C,[12,166,167] where τ_E is linearly dependent on $\bar{n}_e$ for $\bar{n}_e<2\times10^{20}$ m^{-3}. With edge fueling and $\bar{n}_e>2\times10^{20}$ m^{-3}, τ_E saturates. Coincident with the saturation of τ_E is an increasing collisional coupling between the electrons and ions, so that the ion channel becomes more important in determining the total energy confinement. If the ions behaved neoclassically the saturation would occur at higher $\bar{n}_e$, as shown by the solid line. Since it does not, the ion losses are anomalous. A mechanism to explain the anomaly is the ion pressure gradient, or η_i, mode,[138,168–171] which appears when η_i exceeds some critical value $\eta_i^{\rm crit}\approx 1$ to 2. Using $\chi_i^{\rm nc}+\chi_i^{\eta i}$ predicts a reduced T_i peak and narrower T_i profile, which is often more consistent with the experimental results than using constant$\times\chi_i^{\eta i}$.

If the η_i mode is responsible for the anomalous χ_i, then peaking the density profile should reduce η_i, stabilize the η_i mode, reduce χ_i, and increase τ_E. Figure 11 (ALCATOR-C) shows that, with pellet fueling and the ensuing peaked density profiles, τ_E does indeed increase. However, the cessation of sawteeth with pellet fueling has also been proposed as an explanation for this improvement.

If the η_i mode is responsible for the anomalous χ_i, then an ion feature should be observed in the fluctuation spectrum. An ion feature is a turbulence feature propagating in the ion drift direction (in the plasma frame of reference), rather than the electron drift direction. Such a feature has been found[38,41,42,134] in the laboratory frame, but only with poor spatial resolution. Figure 12 shows a comparison of the

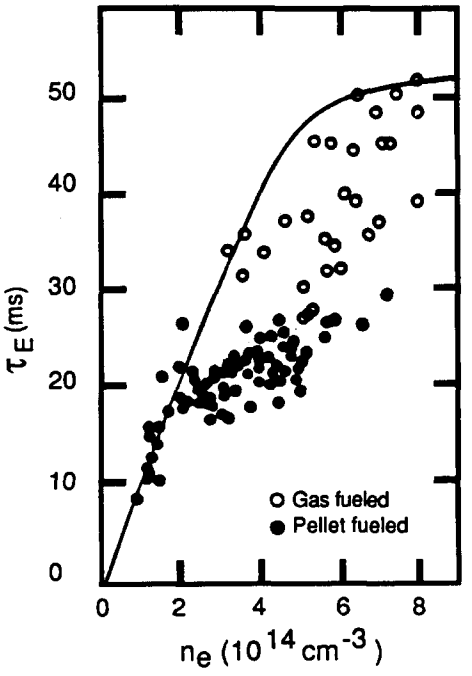

FIG. 11. The global energy confinement time τ_E as a function of density $\bar{n}_e$, from ALCATOR-A[167] ($B_\phi=10$ T, $I_p=750$ kA, H$^+$). Results with both edge fueling (solid circles) and frozen pellet fueling (open circles) are shown. The solid line is the energy confinement time expected using neo-ALCATOR scaling for χ_e and 1×Chang–Hinton (neoclassical) for χ_i.

$S(\omega)$ spectra for three discharges on TEXT, (a) at low density with gas puff fueling, (b) at high density with gas puff fueling, and (c) at high density with pellet fueling.[135] An ion feature (S_i) is seen, whose strength increases as $\bar{n}_e$ increases with gas puff fueling. This could be a signature of the η_i mode. As hoped for, this ion feature is reduced in strength for a pellet fueled (steeper density, reduced η_i) discharge. Unfortunately the TEXT results do not show a clear increase in τ_E or decrease in χ_i when this feature is reduced. We do not yet have sufficient information to use measured

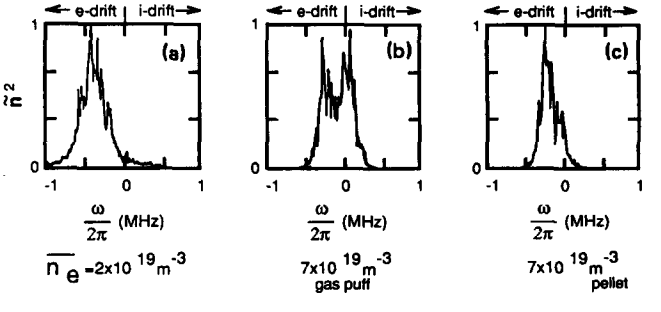

FIG. 12. The power spectrum $S(\omega)$ in arbitrary units for $k_\perp=9$ cm^{-1}, obtained with FIR scattering on TEXT: (a) low-density gas puff ($B_\phi=2.8$ T, $I_p=250$ kA, $\bar{n}_e=3\times10^{19}$ m^{-3}, H$^+$), (b) high-density gas puff ($B_\phi=2.8$ T, $I_p=250$ kA, $\bar{n}_e=6\times10^{19}$ m^{-3}, H$^+$), and (c) high-density pellet fueled ($B_\phi=2.8$ T, $I_p=250$ kA, $\bar{n}_e=6\times10^{19}$ m^{-3}, H$^+$). Negative frequencies correspond to propagation in the electron diamagnetic drift direction.

values of $\tilde{n}/n$ and k (from S_i) in the theoretical expressions for the ion heat fluxes, as we did for drift wave turbulence and electron heat fluxes (e.g., Fig. 9). This comparison is important, because the choice of $\bar{k}_\theta \rho_s$ determines $\chi_i^{\eta_i}$. The exact value of $\bar{v}_{ph}$ for the ion feature also remains to be explained.

IV. MAGNETIC FLUCTUATIONS

A. Coherent MHD activity

Magnetic pick-up loops or Mirnov coils are used to detect the nonaxisymmetric perturbations of the tokamak discharge column. These coils are generally placed outside the plasma, usually at a larger radius than the limiter (often outside the vacuum vessel itself), although on smaller machines these coils have been inserted into the plasma interior. In a tokamak, the plasma may be unstable against a variety of MHD instabilities with poloidal dependencies $\propto \exp[i(m\theta + n\phi)]$, where $m = 0,1,2,...$, and $n = 0,1,2,...$ (m is the poloidal mode number and n is the toroidal mode number, respectively). The mode numbers m and n are found using multiple arrays of coils, and also deduced by measuring the radial decay of the magnetic fields. Because of the spatial decay of the perturbing fields away from the interior resonant surfaces, external sensing coils are most sensitive to the low mode numbers. Early experiments on TOSCA[172] revealed the presence of the expected tearing mode activity, together with a high-frequency component that is discussed further in Sec. IV C. In addition to magnetic coils, soft x-ray imaging systems consisting of a multidetector array of surface barrier detectors are used to interpret oscillations in terms of flux surface perturbations.

Table V lists some of the commonly observed coherent modes, together with their effects on confinement. The central electron temperature is found to rise slowly and fall abruptly in the "sawtooth" pattern.[1,6] Higher frequency resolution of the rising portion of the signal shows the presence of a $m/n = 1/1$ mode just prior to the abrupt temperature fall. The $m/n = 1/1$ mode is thought to cause internal disruptions, in which the region within $r_{q=1}$ is periodically rearranged, sending out heat and density pulses. These pulses are used to demonstrate the diffusive nature of anomalous transport, and also to deduce transport coefficients themselves.[11,24,25] As previously noted, the coefficients so derived are often higher than those derived from a steady-state power balance.

An example of typical soft x-ray signals obtained from TFTR is shown in Fig. 13. Figure 13(a) shows simple sawtooth oscillations;[6] the large $m/n = 1/1$ precursor oscillations are seen clearly on the channel viewing $r = 10$ cm. Small sawteeth [Fig. 13(b)] are similar, but the $m/n = 1/1$ activity is different, there being a large successor oscillation to the crash. Compound sawteeth [Fig. 13(c)] are also found; each compound sawtooth consists of a subordinate relaxation followed by a large (up to 20% in central T_e) main relaxation.

Sawteeth affect confinement properties. For example, there is a mean power flow across a surface of radius r due to the sawteeth[1]

$$q_s(r) = 2\pi R \int p_s(r') 2\pi r' \, dr', \tag{22}$$

with

$$p_s(r) = (W_1 - W_2)/\tau_s, \tag{23}$$

where W_1, W_2 are the energy content per unit volume before and after the crash and τ_s is the sawtooth repetition rate. Further quantified results are found in Refs. 173 and 174. Sawteeth will also affect τ_E by displacing the net power deposition outward; other things being equal this will reduce τ_E. There is also considerable evidence that sawteeth affect both working particle and impurity transport: in particular, they help to counteract a tendency for impurity accumulation on axis.[1]

The usual model[5,175] to explain sawteeth assumes Ohmic heating of T_e in the plasma center, and therefore increasing current density and decreasing safety factor q on axis. When $q(0) < 1$ an $m/n = 1/1$ mode grows, which causes a topological change and a flattening of T_e and a rise in $q(0) > 1$. However, well-documented cases exist in which no correlation between $m/n = 1/1$ activity and the sawtooth crash is found (see, e.g., Ref. 176). Further, evidence is growing that $q(0) < 1$ throughout a sawtooth cycle.[177–179] Theoretical analysis to study the implications of these new experimental results is now initiated. Only recently[179] has it been found that the $m/n = 1/1$ kink mode can be linearly stable for $q(0) < 1$ for certain tailored current profiles.

TABLE V. Coherent magnetic fluctuations and transport.

Mode m/n	Effects	Understanding
1/1	sawteeth?	q profile information needed Is it stochastic or reconnection?
2/1	degrades confinement major disruption	islands decrease effective area
3/2	degrades confinement	islands decrease effective area
4/3, 5/4	small effects on confinement	observed with high beta
m = 10–15	edge transport?	observed close to edge changes with L–H transition

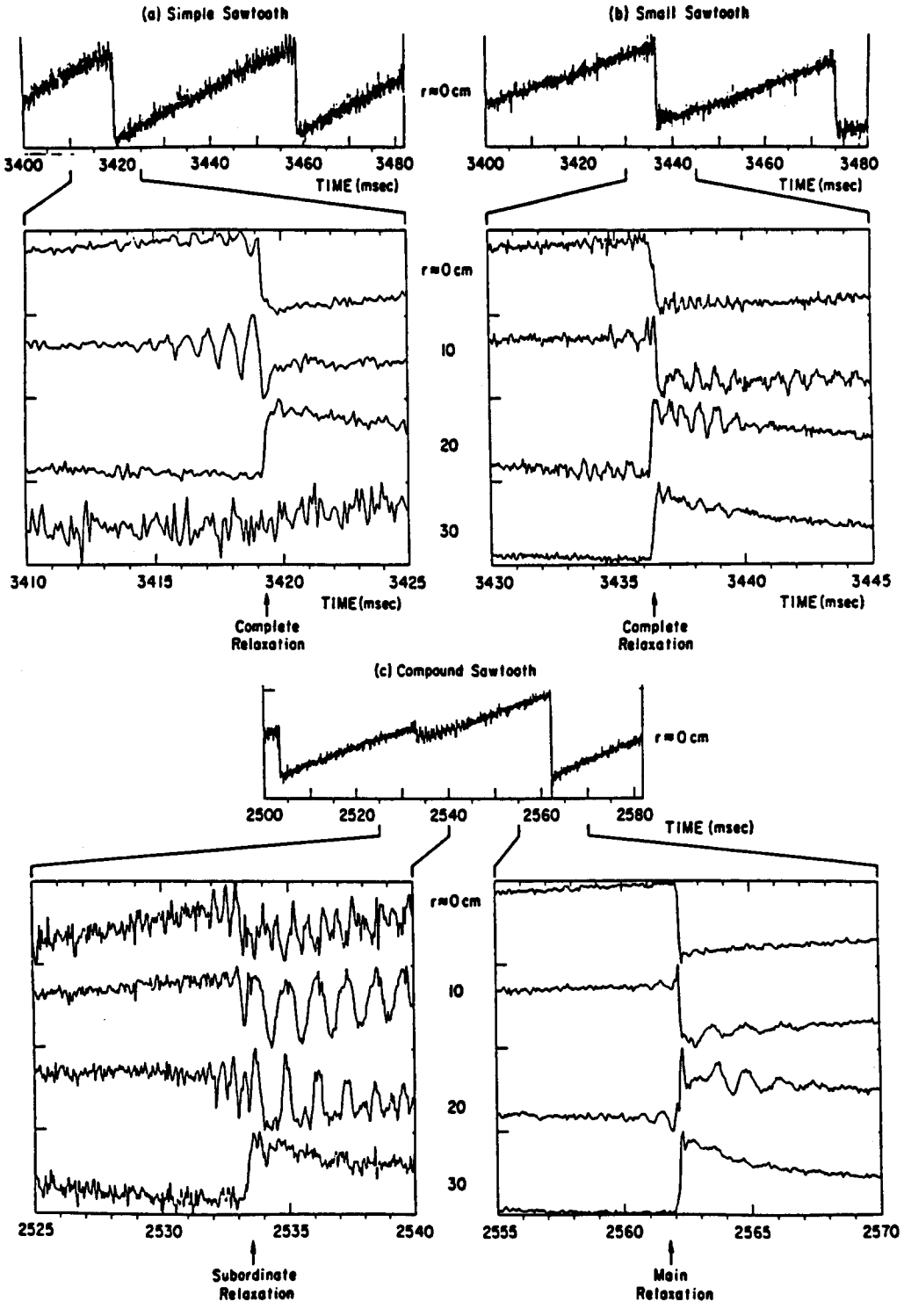

FIG. 13. Soft x-ray signals from TFTR, illustrating three different types of sawtooth activity: (a) Simple sawtooth with an $m/n = 1/1$ precursor, (b) small sawtooth with a continuous $m/n = 1/1$ signal, and (c) compound sawtooth. For each example the signals displayed with expanded timebase illustrate the $m/n = 1/1$ activity.

The stability of the resistive kink modes (or tearing modes) depends on the current profile[180] $j_\phi(r)$ for which there is no direct, external means of control. Nevertheless, for the current profiles that evolve naturally in tokamaks, the $m = 2$, $n = 1$ mode is often the only dangerous and unstable mode. This instability creates a helical "island" structure in the magnetic field that can grow and cause a major disruption of the plasma.[1,181] The disruptive instability is one of the main operational limitations of tokamaks. The theoretical results on kink and tearing mode stability have been taken into account in interpreting observed low-frequency precursor oscillations which have been ascribed to $m = 1$ and $m = 2$ tearing modes for precursors of internal and major disruptions, respectively.[181] The $m = 2$ precursors occur when the radial current distribution is such that there is a slight flattening at the $q = 2$ surface. The $m = 2$ oscillations have been associated with the existence of $m = 2$ magnetic islands, which can increase the radial heat trans-

port enough to cool the plasma interior. An islands of width w at a rational surface r_s cause a transport short circuit across the island[174,182] (no confinement) where it occurs, and

$$\tau_E \approx \tau_{E0}(1 - 4wr_s^2/a^4). \tag{24}$$

The net cross field transport is unchanged; rather the magnetic topology in which the transport occurs is modified. Magnetic islands also increase particle transport.[183,184] Stabilization of the $m = 2$ mode by density control has resulted in factors of 2 improvement in confinement.[185] When the island width reaches a certain level, it causes the onset of the major disruption.

In addition to the $m = 2$ mode, a number of other effects are suspected of contributing to the major disruptions. As an example, nonlinear coupling between the $m = 2$ and the weaker $m = 1$ modes (the latter also being associated with the corresponding $m = 1$ magnetic island) or between the $m = 2$ and the $m = 3$, $n = 2$ mode can lead to large regions of stochastic field lines, which enhances electron thermal transport (see Sec. IV C).

During the initial current rise (e.g., at plasma breakdown) in which skin currents are produced, the tokamak plasma is unstable to modes with $m = 6, 5, 4$, $n = 1$, and Fig. 14 shows an early example of this.[186] The appearance of each mode coincides with the successive occurrence of integral values of $q(r) = m/n = m$ (since $n = 1$). Double tearing modes appear, which allows field line reconnection across the skin current layer, and faster current penetration. Arcs, and an associated impurity influx, can be associated with these periods of instability.

B. High-beta MHD activity

Stable high-deta plasmas are required for the tokamak to attain an economical fusion reactor. Intense neutral beam heating experiments in tokamaks have shown new effects on plasma stability and confinement associated with high beta plasmas. The observed spectrum of MHD fluctuations at high beta is clearly dominated by the $n = 1$ mode when the $q = 1$ surface is in the plasma: this mode does not by itself significantly affect energy confinement.[187] The $m/n = 1/1$ mode drives other $n = 1$ modes through toroidal coupling and $n \geqslant 1$ modes through nonlinear coupling.

From MHD studies performed to date on tokamaks at high beta we can draw a number of conclusions. These are:

(1) The high-beta equilibria obtained to date have reached but not exceeded the ideal beta limit.[188,189]

(2) The observed spectrum of MHD fluctuations at high beta is clearly dominated by the $n = 1$ mode when the $q = 1$ surface is in the plasma. The $m/n = 1/1$ mode is the dominant instability, and it drives other $n = 1$ modes through toroidal coupling and $n \geqslant 1$ modes through nonlinear couplings.

(3) In PDX[190] a resonant interaction of the $n = 1$ internal kink and the trapped fast ions results in loss of beam heating power. Key parameters in the theory are the value of $q(0)$ and the injection angle.

(4) An edge relaxation phenomena or edge localized mode (ERP or ELM) observed during H-mode discharges (e.g., ASDEX,[191] PDX,[192] and D-III[193]) has a dramatic effect on plasma confinement.

(5) Recent studies on TFTR at high-beta poloidal (β_p) show a major disruption limit at $\beta_p \approx 2$ or $\epsilon\beta_p \approx 0.7$, this limit is found to be close the ideal ballooning mode limit calculated from the PEST code.[194]

Tokamak operation at high beta has exhibited an ever richer variety of MHD phenomena. The overall features of the activity are common to all machines. MHD activity continues to limit the range of operating parameters, particularly at the ideal beta limit that has not yet been exceeded on any tokamak. Present results indicate that the beta limit may be defined by the onset of a major disruption. Nevertheless, β optimization techniques are being explored with a low aspect ratio Dee-shaped plasma D-IIID[195] and with a high aspect ratio bean-shaped tokamak with a close fitting shell (PBX-M[196]).

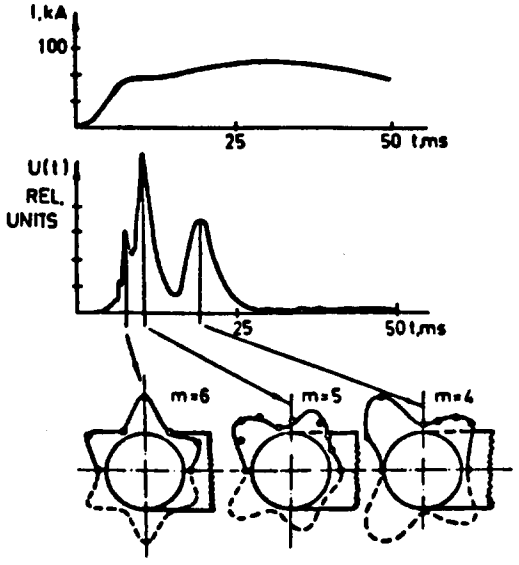

FIG. 14. Coherent MHD modes observed during the plasma current rise phase of T-3.[186]

C. Incoherent MHD activity

Many of the coherent modes described above (except for the $m/n = 1/1$ at reasonably low q values) can be avoided, except perhaps at high β_p values. However, there also exists a broadband magnetic spectrum,[197] in which higher frequencies are associated with higher m numbers. Here we are concerned with the breakup of magnetic surfaces from overlapping magnetic islands. Electron heat transport follows, with any particle transport coming from the associated density fluctuations driven with the magnetic fluctuations. If this mechanism is responsible for transport, then[198] $\chi_e \propto \eta(m_i\beta/m_e)^{1/2}(\alpha/s)^{3/2}$, with $\alpha = -2Rp'/B_\phi^2$ and $s = rq'/q$.

Typically $\tilde{b}/B_\phi \approx 10^{-4}$ to 10^{-5} is measured, with the amplitude increasing towards smaller plasma radius (see Fig. 2). Both high[199–201] and low[76] correlation between the

(edge) electrostatic and magnetic fluctuations is found. It has been suggested that, for Ohmic heating, the measured $\tilde{b}$ is consistent with being a result of $\tilde{n}$ (see Refs. 90 and 202) rather than $\tilde{n}$ being a result of $\tilde{b}$ (see Ref. 203). Table VI lists some of the machines which have studied this broadband spectrum, mostly using coils placed outside the plasma, and attempted to draw conclusions concerning its correlation with plasma transport.

As in the case of density fluctuations, diametrically opposite conclusions have been reached. For example, on Ohmically heated TOSCA[3,106] and additionally heated (L-mode) TFR[152] no correlation between $\tilde{b}$ and confinement properties was found, whereas on Ohmic-heated TCA[204,205] and TOKAPOLE,[54] and additionally heated JET[200] and ISX-B[187,206,207] a clear correlation between increasing $\tilde{b}$ and decreasing energy confinement is found. In ISX-B a prime candidate for this high-frequency activity is high-n resistive ballooning modes. In DIII-D there is a decrease in $\tilde{b}$ at the onset of the H mode; microtearing modes were initially suggested to explain the results,[208] although later stability analysis suggests that this is not the case. Other high-frequency modes have been observed on PDX[190] and D-IIID[193] that may be $n = 2$ to 5 ballooning modes.

Figure 15 shows the results from JET, in which at high values of β_p large increases in $\tilde{b}$ have been seen (see also TOSCA[3,209]). Results from DIII-D, shown in Fig. 16, also demonstrate that the broadband magnetic turbulence is correlated with the quality of confinement. The amplitude

TABLE VI. Incoherent magnetic fluctuations and transport.

ALCATOR-A (212)	Anomalies in SXR signal linked to internal $\tilde{b}/B_\phi$ and considered to explain τ_E.
ASDEX (57)	Increasing interior $\tilde{b}$ (deduced from runaway confinement) is correlated with decreasing confinement (OH to L to H mode).
CALTECH (107)	$\tilde{b}_r$ too small to be important (quasilinear estimate).
DIII and -D (208)	$\tilde{b}$ (5–50 kHz), measured outside plasma, has $m > 8$. $\tilde{b}$ increases with β_p, decreases with increasing τ_E during L–H transition. $\tilde{b}/B_\phi$ for $r \approx a$ (L mode) $\approx 2\times10^{-4}$: quasilinear $\chi_e \sim 2$ m^2 sec^{-1}. Microtearing modes suggested, stabilized for $T > T_{crit}$ in H mode.
DITE (90)	OH: $\tilde{b}_\theta/B_\phi$ at $r = a \propto \bar{n}_e^{-1}$, $m \approx 15$–20, interpreted as generated by filaments in the plasma edge, and interpreted as driven by $\tilde{n}$. ECRH: $\tilde{b}_\theta/B_\phi$ increases by 30% to 200%, largest at low $\bar{n}_e$, related to D_α increase and τ_p decrease.
ISX-B (206,207)	$\tilde{b}/B$ (150 kHz) increases as τ_E decreases for NBI L-mode discharges. Results interpreted in terms of resistive ballooning modes.
JET (200)	$\tilde{b}/B_\phi$ (0–20 kHz) shows broadband turbulent spectrum. Strong correlation along field lines. Two types of fluctuations are found: (a) Edge localized ($\tilde{b}$, $\tilde{n}$ well correlated) with m, n increasing with frequency up to $m \sim 100$. These are correlated with confinement: $\lvert\tilde{b}\rvert q(a) \sim \tau_E^{-1}$. Here, χ_e near the edge is consistent with $\tilde{b}$ if the strong turbulence model is used, with $L_{ac} \sim \delta_l \sim (\tilde{b}_r/B_\phi)^{-1}$. (b) With high power or low $q(a)$, standing waves with $n \sim 1$, $m \sim q(a)$ dominate above 10–15 kHz. Edge localized fluctuations of disruptive type nature appear just before L–H transition. Transitions back to the L phase are marked by long toroidal wavelength ($n \sim 1$) broadband activity.
MACROTOR (76,78)	$\tilde{b}_r/B_\phi$ increases with decreasing r, to 10^{-4} at $r/a = 0.6$, too small to explain transport using quasilinear expression. No dependence of $\tilde{b}_r/B_\phi$ on n (and therefore τ_E), or MHD mode amplitude. $\tilde{n}$ and $\tilde{b}$ uncorrelated.
TCA (204,205)	$\tilde{b}_r \sim \tilde{b}_\theta$ but uncorrelated above 100 kHz $\tilde{b}$ depends on $d\bar{n}_e/dt$ and dI_p/dt. Direct correlation between τ_E and high frequency $\tilde{b}/B_\phi$ found for OH discharges: $\tilde{b}$ is related to interior plasma.
TEXT (141,199)	Internal $\tilde{b}$ too small to account for edge transport if quasilinear formulas applied, although $\tilde{b} \propto \tau_E^{-1}$. Correlations found between $\tilde{n}$ and $d\tilde{b}/dt$ for $\tilde{b}(r > a)$, $\tilde{n}(r < a)$. Quasilinear expressions shown to apply for χ_e for externally applied $m \sim 7$ stochastic fields.
TFR (152)	No correlation between $\tilde{b}$ and τ_E found for OH or additional heating.
TFTR (65)	$\tilde{b}_\theta/B_\phi$ at wall increases with NBI to 2×10^{-5}, $m > 15$. $\tilde{b}$ affected by gas puffing, impurities (laser ablation) and coherent MHD.
TM-3 (197)	Measurements of broadband $\tilde{b}$ at the wall.
TOSCA (3,79,106,172,209)	No correlation of internal $\tilde{b}_r/B_\phi$ ($\sim 10^{-5}$) in 100–200 kHz range and τ_E, except at high β, where conduction from stochasticity is important. $\tilde{b}/B_\phi$ too small to explain τ_E in OH plasma (quasilinear formula). Removing residual low m/n (Mirnov) activity with external coils reduces incoherent $\tilde{b}$ without affecting confinement. $\tilde{b}$ is due to $\tilde{n}$, not other way.
TOKAPOLE (54)	$\tilde{b}_\theta \approx 2\tilde{b}_r \approx 10\tilde{b}_\phi$ measured internally increases towards center, increases as $q(a)$ decreases. $\tilde{b}$ too small to explain τ_E except for $q(a) < 1$.

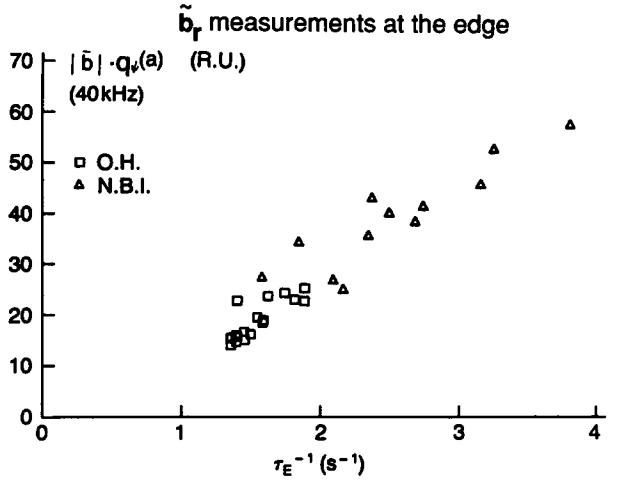

FIG. 15. The relationship between $\tilde{b}_\theta q(a)$ and energy confinement time τ_E obtained on JET,[200] for Ohmic and neutral beam injected (NBI) plasmas.

changes abruptly at the transition between various modes of confinement: Ohmically heated, L mode, H mode, and during ELM's (edge localized modes). The fluctuation amplitude is largest where the separatrix intersects the divertor plates, which is interpreted as evidence for the existence of line tied image currents in the scrape off later, beyond the separatrix. However, there is a problem with interpreting these transitions as being solely due to changes in $\tilde{b}$. The different modes (L and H) refer to particle as well as electron energy confinement, and magnetic stochasticity is not expected to significantly influence particle transport.

Studies of the high-frequency broadband magnetic spectrum on TFTR and TCA[204] show that the amplitude level is extremely sensitive to local edge boundary conditions. Results on FT[210] show sensitivity to plasma position. These findings may partially explain why different machines obtain different results for the correlation between τ_E and $\tilde{b}$.

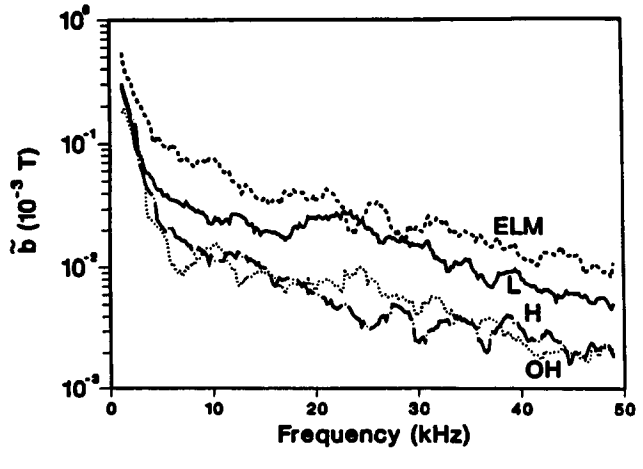

FIG. 16. The frequency spectra of the magnetic fluctuations in DIII-D at the outer divertor hit spot for Ohmical heated (OH), low confinement (L), high confinement (H), and during periods with edge localized modes present (ELM).

Quantitative calculations of the effects of the measured $\tilde{b}$ are difficult. First it must be decided if the (usually) externally measured $\tilde{b}$ represents edge or interior phenomena. Different conclusions have been reached concerning this point. The measured $\tilde{b}$ must be extrapolated to the value of $\tilde{b}$ at the resonance surfaces, a check made to ensure island overlap has occurred, and then a formula chosen to infer local electron heat transport. To explain χ_e using the quasilinear expression, [Eq. (9)] $\tilde{b}_r/B_\phi$ must decrease from $\approx 1\times 10^{-3}$ at the periphery to $\approx 1\times 10^{-4}$ near the center, whereas limited results show the opposite radial dependence, i.e., experimentally $\tilde{b}_r/B_\phi$ increases with decreasing radius. Unless strong turbulence formulas are invoked (c.f. JET[200]), it is usually true that $\tilde{b}$ is too small to produce significant energy fluxes using existing models and formulae, except at high β values.[3] Externally generated magnetic stochasticity produces an electron heat flux consistent with the quasilinear result.[211]

Other (than coil) diagnostics have been used to infer internal magnetic structure. On ALCATOR-A, anomalies in the soft x-ray spectrum were interpreted in terms of $\tilde{b}$ and this was considered to explain the internal electron heat fluxes.[212] The ratio of runaway to thermal energy confinement has also been used to infer internal magnetic structure.[55-57] Runaway confinement is improved over thermal confinement because of the phase averaging over magnetic perturbations when the drift surfaces are displaced from the magnetic surfaces. On ASDEX[57] a correlation between degraded τ_E and increasing internal $\tilde{b}$ (deduced from runaway electron confinement) is claimed. Other evidence that magnetic stochasticity is playing a role in transport comes from measurements of plasma potential Φ; at low densities[213] $\Phi(a) > 0$ and this has been interpreted as being caused by electron loss to a limiter across stochastic magnetic fields. Externally imposed stochastic layers[164] clearly increase the edge plasma potential Φ and electric field E_r.

To draw any conclusions concerning the role of $\tilde{b}$ in determining interior confinement is impossible, except perhaps to say that there is generally little correlation between τ_E and $\tilde{b}$ in Ohmic discharges (exception, TCA, TOKAPOLE), and more of a correlation as β_p is increased. As in the case of density fluctuations, spatial asymmetries, the choice of turbulence model, the location of the $\tilde{b}$ signal, and other variable plasma parameters might account for the many different observations. Clearly localized, internal measurements of $\tilde{b}$ in a tokamak are required if further progress is desired.

V. THE ROLE OF NONTOKAMAKS

To this point this review has dealt solely with experimental results from tokamaks, most of "medium size." Many other machines, not just tokamaks, can contribute to the understanding of the role of fluctuations in tokamak transport.

First small tokamaks, which usually fit the same global scaling laws that describe transport in large tokamaks,[214] can utilize material probes across almost all of the cross section. This allows a measurement of fluctuation-driven con-

duction and convection energy fluxes. Examples of the importance of using small tokamaks for fluctuation studies are found in the work on TOSCA,[3] MACROTOR,[78] and TOKAPOLE.[54] Small machines can also be used to develop both diagnostic and analysis techniques.

Linear machines have successfully and elegantly demonstrated that modes can be isolated, controlled, and the mode growth and saturation, and ensuing transport, measured. In particular, various drift instabilities have been studied (e.g., Ref. 215 and references therein, and Ref. 216). Such experiments allow tests of theoretical models in conditions where all relevant parameters can be measured and often controlled, and also in conditions that are simpler to model theoretically than a tokamak. This allows detailed checks on models and mathematical formalisms before they are applied to the much more complicated case of a tokamak.

Reversed field pinches and stellarators (or torsatrons) offer the opportunity to compare correlations between fluctuations and transport in different magnetic geometries.[64] We can empirically seek similarities and differences in turbulence and transport, and in magnetic structure, and perhaps gain insight into the important parameters determining the turbulence itself. Alternatively, we can invoke theory to predict the "ratio" of turbulence and transport between machines for various modes. By measuring the turbulence and transport properties and comparing them with the theoretical predictions we can then gain insight into whether a particular (theoretical) mode is really present. Tokamaks, stellarators, and pinches should suffer drift wave turbulence and transport, which can perhaps be modified by ECRH control of trapped electron populations.[3] The reversed field pinches exhibit large levels of magnetic turbulence, and therefore offer a good test bed for developing internal magnetic fluctuation diagnostics. Edge turbulence on tokamaks and HELIOTRON-E (a torsatron) has very similar properties,[96] perhaps suggesting a common and noncurrent-driven driving term.

VI. FUTURE DIRECTIONS

Table VII summarizes an approach to a further understanding of tokamak turbulence, and the role it plays in determining plasma transport properties. At the plasma edge a clear relationship has been found between the measured fluctuation levels, and the transport. However, asymmetries must be studied further. In the interior any relationship between transport and fluctuations is much harder to demonstrate, because we do not have, and are unlikely to have, all the necessary correlations. Instead we will have to rely on testing various models, being careful that spatial asymmetries are looked for and if present accounted for. Many problems arise, and some are noted at the bottom of the table. Of particular concern is the possibility that different modes coexist, that different modes appear and disappear with different conditions, and lastly that different modes will appear in the presence of significant alpha particle production.

Insight into the underlying turbulence mechanisms can also be gained by studying the transport coefficients D and χ, or the fluxes Γ and q, themselves. Scaling laws, cast in the correct variables, provide information on the basic physical processes.[198] The ratio of χ to D may uniquely determine a type of turbulence.[1,27,217] These techniques can be complicated if more than one mode exists.

Diagnostic development is required. First, $\tilde{n}$ must be measured with good spatial and wave number (k) resolution: we must be able to distinguish individual characteristics of simultaneously occurring turbulence features. Either a new diagnostic, a modified correlation technique applied to HIBP data, or simultaneous operation of HIBP and heter-

TABLE VII. An approach to understanding turbulence.

1. **Characterize fluctuations** in terms of global, local, and *dimensionless* parameters. This may rule out certain possibilities, and tell us which turbulence regime we are in (quasilinear, strong).
E.g., $\omega \sim \omega_{*_e}$ rules out Alfvén waves; and $\tilde{n}/n \sim$ mixing length estimate and $\Delta\omega/\omega \sim 1$ rules out quasilinear regime (?)

2. **Find the driving terms** (∇n, ∇T, ∇j, ∇v).
E.g., does the turbulence remain unchanged as the very flat density profiles of the DIII-D H mode is entered? (implies driving term not ∇n)
Does the turbulence remain the same when $j \Rightarrow 0$, by current ramping or in a stellarator? (implies driving term not ∇j).

3. **Demonstrate causality between fluctuations and transport**
Test theoretical models (some ruled out by now), allowing for possible spatial asymmetries.

4. **Test models by scaling**

5. **Reduce fluctuations and improve (?) confinement**
(a) change magnetic geometry
(b) reduce driving terms
(c) increase damping terms
(d) feedback stabilize, either partial (suppress dominant modes only, allowing others driving less transport to grow) or complete
(e) dynamically stabilize
(f) modify distribution functions

PROBLEMS
How do we cope if:
(a) different modes coexist?
(b) new phenomena appear with changing conditions (e.g., when trying to change driving terms, or with alpha particles)?
(c) local turbulence characteristics cannot distinguish between different modes?

odyne FIR scattering, should be considered. Diagnostics to measure internal $\tilde{T}$ and $\tilde{b}$ should be developed. More use of existing analysis techniques is recommended.

VII. SUMMARY AND CONCLUSIONS

To preface this section, we must remark that there is at least one exception to almost every statement made.

In the edge plasma ($\rho > 0.8$) detailed measurements of the various fluctuating quantities density $\tilde{n}$, potential $\tilde{\phi}$, temperature $\tilde{T}$, and magnetic field $\tilde{b}$, together with the various correlations, have been made. The turbulence is broadband ($\Delta\omega/\bar{\omega}$, $\Delta k_\theta/\bar{k}_\theta > 1$) with frequency $\bar{\omega}/2\pi \approx 100$ kHz, a mean poloidal wave number $\bar{k}_\theta \approx 200\ \mathrm{m}^{-1}$, a mean radial wave number $\bar{k}_r \approx 0$, and parallel wave number $\bar{k}_\parallel \approx 1\ \mathrm{m}^{-1}$. The ratio of half-widths $\sigma(k)$ of the $S(k_r,k_\theta)$ spectrum is $\sigma(k_r)/\sigma(k_\theta) \approx 2$, and $\sigma(k_\parallel) \approx \bar{k}_\parallel$. Typical fluctuation levels are $\tilde{n}/n \approx 0.2$, $\tilde{\phi}/(k_b T_e) \approx 0.3$, $\tilde{T}_e/T_e < 0.1$, and $\tilde{b}_r/B_\phi \approx 1 \times 10^{-5}$.

The measurements allow the fluctuation-driven particle and heat fluxes to be derived and compared with the total fluxes. Where measured, the electrostatic turbulence is responsible for a large part, if not all, of the edge particle flux. Here, Γ^i and $\Gamma^{f,E}$ agree in both amplitude (within a factor ~ 2) and scaling with parameters (B_ϕ, I_p, $\bar{n}_e$, impurity content, E_r). The role of the measured asymmetries should be further investigated. The energy fluxes are less well accounted for by the electrostatic fluctuations, but the error bars are large. It is possible that with $\bar{n}_e > 3 \times 10^{19}\ \mathrm{m}^{-3}$ the electrostatic fluctuations do account for all the energy flux, with convection the dominant term. At lower densities nonthermal electrons may play a role by increasing the parallel heat flux to the limiter. If there is an unaccounted energy flux, and the particle flux is already well explained, then this unaccounted energy flux must be explained by a process that does not significantly affect particle fluxes (e.g., $\tilde{b}$). In Ohmic-heated low-β plasmas the measured $\tilde{b}$, interpreted using a quasilinear formula, is too small to contribute to the thermal losses.

The edge turbulence is well characterized, but no completely satisfactory model has been found that predicts all the measured features. The least problematic is the resistivity gradient model, which fails only in its prediction of the m numbers. An up-down asymmetry has been isolated, perhaps a result of toroidal asymmetries, for example the limiter or the discrete toroidal field coils.

In the plasma confinement region fluctuation measurements are presently restricted to $\tilde{n}$, $\tilde{\phi}$, and their correlations. Three distinct features are observed. First is the broadband turbulence, with characteristics similar to those at the edge. Both $\tilde{n}/n$ and $\tilde{\phi}/(k_b T_e)$ decrease toward the plasma center, and $\bar{k}_\theta \rho_s \approx 0.1$ to 1 (but with caveats on the interpretation of $\bar{k}$ because of the possible presence of an ion feature). The fluctuations propagate in the electron diamagnetic drift direction. This feature is often attributed to drift wave turbulence and invoked to explain experimental q_e. Second, quasicoherent modes have been identified at the high toroidal field side of the plasma. Again, these features propagate in the electron diamagnetic drift direction. No theoretical explanation exists, but they are drift-wave like. Third, at high densities, a broadband feature propagating in the ion drift direction is found, which has been associated with the ion pressure gradient-driven, or η_i, mode. This mode is used to explain χ_i which in turn is invoked to explain the saturation of τ_E at high densities.

Clearly the spatial dependence of the fluctuations is complicated. This fact, and the theoretically expected complicated relationship between $\tilde{n}/n$ and a flux or transport coefficient, means that we should not necessarily expect to find a simple relationship between a line of sight or single point measurement of $\tilde{n}/n$ and a plasma transport coefficient or a flux.

The characteristics of the observed fluctuations have been compared with the predictions of the models suggested to explain them. We have also compared the measured plasma transport properties with those predicted to result from the modes, using where possible, measured turbulence properties. We find:

(1) There is broad agreement between $(\tilde{n}/n)^{\mathrm{exp}}$ and $(\tilde{n}/n)^{\mathrm{slab}}$ if the results from many machines are plotted on a log–log scale.[4] However, a careful analysis of results from individual machines shows significant departures. On TEXT, where good spatial resolution is obtained using the HIBP, the broadband fluctuation levels are well represented by mixing length estimates only for $\rho > 0.5$, where $(\tilde{n}/n)^{\mathrm{slab}}$ is within a factor ~ 2 of $(\tilde{n}/n)^{\mathrm{exp}}$. Choosing $\bar{k}_\theta \rho_s \approx 0.4$ (instead of the measured 0.1) brings $(\tilde{n}/n)^{\mathrm{tor}}$ within a factor ~ 2 of $(\tilde{n}/n)^{\mathrm{exp}}$. Neither model predicts the measured $(\tilde{n}/n)^{\mathrm{exp}} \approx 0.01$ at $\rho = 0$ (where the measurements of scale lengths are difficult). The problems of data interpretation in the presence of counterpropagating turbulence are important in this comparison.

(2) $\bar{k}_\theta \rho_s \approx$ const, a convenient assumption, is not generally found; as for point (1) above, the problems associated with the presence of counterpropagating turbulence are important in making this determination. While there is evidence for the expected B_ϕ dependence of $\bar{k}_\theta$, there is very little evidence for the T_e or mass dependence.

(3) The slab collisional, universal, and dissipative trapped electron drift wave modes are, respectively, stable, stable, and unstable at the measured k_θ values.

(4) The broadband feature, interpreted as quasilinear drift wave turbulence, does not explain the usual description of interior particle transport. No large inward pinch velocity is predicted. However, limitations in the measurements of both total and fluctuation driven particle flux should be recognized.

(5) The broadband feature, interpreted as quasilinear drift wave turbulence, does not consistently explain the measured interior electron heat flux. This is in contrast to predictive code calculations: the difference lies in the assumed and measured values of $\tilde{n}/n$ and $\bar{k}_\theta$. The experimental values are uncertain because of the problems associated with data interpretation in the presence of counter propagating turbulence. While the choice of working ion affects q_e^{tot}, it does not affect q_e^{dw} for the model considered. To continue this (and the particle flux) model and experiment comparison, it is

important to understand and correctly interpret the effects of any ion feature. More detailed measurements of $\bar{k}$ are required. Obviously other models, both drift wave and anything else, should be tested in a similar manner.

(6) The measured ion temperatures are often approximately predicted using the sum of the neoclassical and pressure gradient-driven ion thermal fluxes. The measured ion feature suggests the presence of the ion pressure gradient-driven mode. The characteristics of the ion feature should be further investigated (e.g., the spatial localization, the scalings of $\tilde{n}/n$ and $\bar{k}$).

Coherent magnetic fluctuations are comparatively well understood. However, the role of the $m/n = 1/1$ mode in determining sawtooth activity, and the value of $q(0)$ during a sawtooth, is not clear. The sawteeth themselves appear to drive additional density fluctuations, which might explain the high transport coefficients deduced from sawtooth propagation. High-frequency (~ 1 MHz) turbulence is also associated with the sawtooth collapse: this may play a role in understanding the sawtooth process itself.

The incoherent magnetic fluctuations, like the density fluctuations, have been found both to correlate and not to correlate with plasma transport. They are broadband, increasing with decreasing minor radius. Better correlation between increasing $\tilde{b}$ and decreasing τ_E is found as β increases. A correlation between $\tilde{b}$ and the quality of confinement is found during various transitions to regimes of different confinement (OH, L-mode, H-mode, and ELM's). However, it is not generally expected that a changing $\tilde{b}$ alone can explain the particle transport changes that occur at these transitions.

As in the case of density fluctuations, we should perhaps not expect to find a simple correlation with our present diagnostics, even if $\tilde{b}$ is responsible for transport. Time derivatives of plasma parameters are known to markedly affect $\tilde{b}$, which further complicates any comparisons. It is important to measure internal $\tilde{b}$, and to know which formula to use to deduce an electron heat flux. In small machines, where internal $\tilde{b}$ has been measured, it is too small [except at very low $q(a)$] to account for a significant energy flux when interpreted using the quasilinear formula. We must answer the question: is the measured $\tilde{b}$ simply a response to the measured $\tilde{n}$?

Turning to recommendations for future work, an obvious area is in improved diagnostics. In particular, diagnostics should be developed to measure $\tilde{T}_e$ and $\tilde{b}$ inside the plasma. The likely amplitudes (small) and frequencies must be recognized before implementing proposed systems. At the same time, better use of existing statistical analysis techniques should be made. In particular, we need to include k information in higher-order analysis, and to use nonstationary techniques to follow the effects of transients. It is also important to obtain $\tilde{n}$ information with good spatial and k resolution. The problems of interpreting the HIBP data should be addressed either by advanced statistical techniques, or by studying a discharges without an ion feature. Once a suitable ion-mode-free discharge is found, or HIBP analysis capable of distinguishing such a feature is available, it is important to measure the value and scaling of $\bar{k}_\theta$. This is because of its importance in determining the quasilinear fluxes. However, other (strong turbulence, stochastic) expressions should also be made available for comparison.

While we are presently concentrating on understanding the effects of turbulence on working particle and energy transport, we should not forget to study the effects on momentum and impurities. Impurity transport plays a determining role in steady-state operation.

The role that small tokamaks and nontokamaks can play in the understanding of tokamak transport should not be overlooked, both in the development of new diagnostics and analysis techniques, testing our turbulence models in more controlled plasmas, and in allowing comparisons of results in differing magnetic geometries.

Lastly, it is emphasized that to "understand" turbulence represents a long-term objective. It is unlikely that we will ever have sufficient confidence in theoretical models to use the predicted transport coefficients in a predictive code to design future machines. As such, empirical characterizations of fluctuations and local transport properties, and scaling laws will always play an important role.

[1] J. Hugill, Nucl. Fusion **23**, 331 (1983).
[2] P. C. Liewer, Nucl. Fusion **25**, 543 (1985).
[3] D. C. Robinson, in *Turbulence and Anomalous Transport in Magnetized Plasmas*, Cargese Workshop 1986, edited by D. Gresillon and M. Dubois (Ecole Polytechnique, Palaiseau, France, 1986), p. 21.
[4] C. M. Surko, in *Turbulence and Anomalous Transport in Magnetized Plasmas*, Cargese Workshop 1986, edited by D. Gresillon and M. Dubois (Ecole Polytechnique, Palaiseau, France, 1986), p. 93.
[5] J. A. Wesson, P. Kirby, and M. F. Nave, in *Plasma Physics and Controlled Nuclear Fusion Research 1986*, Kyoto (IAEA, Vienna, 1987), Vol. 2, p. 3.
[6] S. Von Goeler, W. Stodiek, and N. Sauthoff, Phys. Rev. Lett. **33**, 1201 (1974).
[7] K. W. Gentle, Nucl. Technol./Fusion **1**, 479 (1981).
[8] B. Coppi and N. Sharky, Nucl. Fusion **21**, 1363 (1981).
[9] D. W. Ross, Comm. Plasma Phys. Controlled Fusion **XII**, 155 (1989).
[10] K. W. Gentle, B. Richards, and F. Waelbroeck, Plasma Phys. Controlled Fusion **29**, 1077 (1987).
[11] S. K. Kim *et al.*, in *Plasma Physics and Controlled Nuclear Fusion Research, 1988*, Nice (IAEA, Vienna, 1989), Vol. 1, p. 281.
[12] M. Greenwald *et al.*, in *Plasma Physics and Controlled Nuclear Fusion Research 1986*, Kyoto (IAEA, Vienna, 1987), Vol. 1, p. 139.
[13] B. B. Kadomtsev and O. P. Pogutse, Nucl. Fusion **11**, 67 (1971).
[14] F. L. Hinton and R. D. Hazeltine, Rev. Mod. Phys. **48**, 239 (1976).
[15] Yu. N. Dnestrovskii, S. V. Neudachin, and G. V. Pereverzev, Sov. J. Plasma Physics **10**, 137 (1984).
[16] Yu. F. Baranov *et al.*, Sov. J. Plasma Phys. **13**, 455 (1987).
[17] N. L. Vasin, E. P. Gurbunov, S. V. Neudachin, and G. V. Pereverzev, Sov. J. Plasma Phys. **8**, 133 (1982).
[18] R. C. Isler, Nucl. Fusion **24**, 1599 (1984).
[19] G. M. McCracken and P. E. Stott, Nucl. Fusion **10**, 889 (1979).
[20] A. J. Wootton, J. Vac. Sci. Technol. A **4**, 1918 (1986).
[21] K. McGuire *et al.*, Plasma Phys. Controlled Fusion **30**, 1391 (1988).
[22] W. M. Stacey, C. M. Ryu, and M. A. Malik, Nucl. Fusion **26**, 293 (1986).
[23] M. Bitter *et al.*, Plasma Phys. and Controlled Fusion **29**, 1235 (1987).
[24] E. D. Fredrickson *et al.*, Nucl. Fusion **26**, 849 (1986).
[25] B. J. D. Tubbings, N. J. Lopes Cardozo, and M. J. Van der Wiel, Nucl. Fusion **27**, 1843 (1987).
[26] R. J. Groebner *et al.*, Nucl. Fusion **26**, 543 (1986).
[27] A. Gondhalekar, A. D. Cheetham, J. C. M. DeHaas, A. Hubbard, J. O'Rourke, and M. L. Watkins, Plasma Phys. Controlled Nucl. Fusion **31**, 805 (1989).
[28] R. J. Bickerton, Nucl. Fusion **13**, 290 (1973).
[29] M. C. Zarnstorff and the TFTR group, in *Plasma Physics and Controlled*

Nuclear Fusion Research 1988, Nice (IAEA, Vienna, 1989), Vol. 1, p. 183.
[30] E. J. Powers, Nucl. Fusion **14**, 749 (1974).
[31] Equipe TFR, Nucl. Fusion **18**, 647 (1978).
[32] *Diagnostics for Fusion Reactor Conditions*, Proceedings of Workshop, Varenna 1982 (CEC, Brussels, 1982), Vols. 1 and 2.
[33] N. C. Luhmann, Jr. and W. A. Peebles, Rev. Sci. Instrum. **55**, 279 (1984).
[34] D. V. Orlinski and G. Magyar, Nucl. Fusion **28**, 611 (1988).
[35] D. E. Smith, E. J. Powers, and G. S. Caldwell, IEEE Trans. Plasma Sci. **PS-2**, 261 (1974).
[36] Ch. P. Ritz *et al.*, Rev. Sci. Instrum. **9**, 1739 (1988).
[37] J. Sheffield, in *Plasma Scattering of Electromagnetic Radiation* (Academic, New York, 1975).
[38] D. L. Brower, W. A. Peebles, and N. C. Luhmann, Jr., Nucl. Fusion **27**, 2055 (1987).
[39] Ch. P. Ritz, R. D. Bengtson, S. J. Levinson, and E. J. Powers, Phys. Fluids **27**, 2956 (1984).
[40] D. L. Brower, W. A. Peebles, S. K. Kim, and N. C. Luhmann, Jr., Rev. Sci. Instrum. **9**, 1559 (1988).
[41] D. L. Brower *et al.*, Phys. Rev. Lett. **59**, 48 (1987).
[42] K. Kawahata *et al.*, in *Plasma Physics and Controlled Nuclear Fusion Research 1988*, Nice (IAEA, Vienna, 1989), Vol. 1, p. 287.
[43] P. Schoch *et al.*, Rev. Sci. Instrum. **9**, 1646 (1988).
[44] G. H. Hallock, A. J. Wootton, and R. L. Hickok, Phys. Rev. Lett. **59**, 1301 (1987).
[45] J. M. Beall, Y. C. Kim, and E. J. Powers, J. Appl. Phys. **53**, 3933 (1982).
[46] T. Lehecka *et al.*, Rev. Sci. Instrum. **9**, 1620 (1988).
[47] C. Hidalgo, A. P. Navarro, M. A. Pedrosa, and L. Rodriguez, in *Proceedings of the 15th European Conference on Controlled Fusion and Plasma Physics* (European Physical Society, Petit-Lancy, Switzerland, 1988), Vol. 1, p. 199.
[48] J. M. Senties *et al.*, in *Proceedings of the 16th European Conference on Controlled Fusion and Plasma Physics* (European Physical Society, Petit-Lancy, Switzerland, 1989), Vol. 1, p. 51.
[49] P. Cripwell, A. E. Costley, and A. E. Hubbard, in *Proceedings of the 16th European Conference on Controlled Fusion and Plasma Physics* (European Physical Society, Petit-Lancy, Switzerland, 1989), Vol. 1, p. 75.
[50] T. Lehecka *et al.*, in *Proceedings of the 16th European Conference on Controlled Fusion and Plasma Physics* (European Physical Society, Petit-Lancy, Switzerland, 1989), Vol. 1, p. 123.
[51] S. J. Zweben, J. M. Chesney, and R. W. Gould, Nucl. Fusion **23**, 825 (1983).
[52] A. Cavallo and R. Cano, Plasma Phys. **23**, 61 (1981).
[53] TFR Group, in *Proceedings of the 9th European Confernece on Controlled Fusion and Plasma Physics* (European Physical Society, Petit-Lancy, Switzerland, 1979), Vol. 1, p. 17.
[54] D. E. Graessle, S. C. Prager, and R. N. Dexter, Phys. Rev. Lett. **62**, 535 (1989).
[55] H. E. Mynick and J. A. Krommes, Phys. Rev. Lett. **43**, 1506 (1979).
[56] H. E. Mynick and J. D. Strachan, Phys. Fluids **24**, 695 (1981).
[57] O. J. Kwon *et al.*, Nucl. Fusion **28**, 1931 (1988).
[58] T. P. Crowley, Rev. Sci. Instrum. **9**, 1638 (1988).
[59] P. M. Schoch *et al.*, in *Proceedings of the 16th European Conference on Controlled Fusion and Plasma Physics* (European Physical Society, Petit-Lancy, Switzerland, 1989), Vol. 2, p. 525.
[60] W. Horton, D.-I. Choi, P. N. Yushmanov, and V. V. Parail, Plasma Phys. Controlled Nucl. Fusion **29**, 901 (1987).
[61] P. Grassberger and I. Procaccia, Physica **9D**, 189 (1983).
[62] A. Cote, P. Haynes, A. Howling, A. W. Morris, and D. C. Robinson, in *Proceedings of the 12th European Conference on Controlled Fusion and Plasma Physics* (European Physical Society, Petit-Lancy, Switzerland, 1985), Vol. 2, p. 450.
[63] W. Arter and D. N. Edwards, in *Proceedings of the 12th European Conference on Controlled Fusion and Plasma Physics* (European Physical Society, Petit-Lancy, Switzerland, 1985), Vol. 2, p. 442.
[64] A. A. Howling, A. W. Morris, and D. C. Robinson, in *Proceedings of the 1985 Cargese Workshop on Magnetic Reconnection and Turbulence*, edited by D. Gresillon and M. Dubois (Ecole Polytechnique, Palaiseau, France, 1985), p. 329.
[65] S. J. Zweben *et al.*, J. Nucl. Mater. **144–147**, 250 (1987).
[66] H. Johnsen, H. L. Pecseli, and J. Trulsen, Phys. Fluids **30**, 2239 (1987).
[67] J. D. Strachan *et al.*, Nucl. Fusion **22**, 1145 (1982).
[68] E. Holzhauer *et al.*, in *Turbulence and Anomalous Transport in Magnetized Plasmas*, Cargese Workshop 1986, edited by D. Gresillon and M. Dubois (Ecole Polytechnique, Palaiseau, France, 1986), p. 137.
[69] Ch. P. Ritz *et al.*, Nucl. Fusion **27**, 1125 (1987).
[70] A. Cote and D. E. Evans, in *Turbulence and Anomalous Transport in Magnetized Plasmas*, Cargese Workshop 1986, edited by D. Gresillon and M. Dubois (Ecole Polytechnique, Palaiseau, France, 1986), p. 111.
[71] R. A. Koch and W. M. Tang, Phys. Fluids **21**, 1236 (1978).
[72] S. J. Zweben and S. S. Medley, Phys. Fluids B **1**, 2058 (1989).
[73] S. J. Zweben and R. W. Gould, Nucl. Fusion **23**, 1625 (1983).
[74] S. J. Zweben, P. C. Liewer, and R. W. Gould, J. Nucl. Mater. **111 and 112**, 39 (1982).
[75] P. Liewer, J. M. Chesney, S. J. Zweben, and R. W. Gould, Phys. Fluids **29**, 309 (1986).
[76] S. J. Zweben and R. J. Taylor, Nucl. Fusion **21**, 193 (1981).
[77] S. J. Zweben and R. J. Taylor, Nucl. Fusion **23**, 513 (1983).
[78] S. J. Zweben, C. R. Menyuk, and R. J. Taylor, Phys. Rev. Lett. **42**, 1270 (1979).
[79] A. A. Howling and D. C. Robinson, in *Turbulence and Anomalous Transport in Magnetized Plasmas*, Cargese Workshop 1986, edited by D. Gresillon and M. Dubois (Ecole Polytechnique, Palaiseau, France, 1986), p. 115.
[80] A. Howling, A. Cote, E. J. Doyle, D. E. Evans, and D. C. Robinson, in *Proceedings of the 12th European Conference on Controlled Fusion and Plasma Physics* (European Physical Society, Petit-Lancy, Switzerland, 1985), Vol. 1, p. 311.
[81] A. A. Howling and D. C. Robinson, Plasma Phys. Controlled Fusion **30**, 1863 (1988).
[82] S. J. Levinson, J. M. Beall, E. J. Powers, and R. D. Bengston, Nucl. Fusion **24**, 527 (1984).
[83] W. L. Rowan *et al.*, Nucl. Fusion **27**, 1105 (1987).
[84] Ch. Ritz *et al.*, Phys. Rev. Lett. **62**, 1844 (1989).
[85] Ch. P. Ritz *et al.*, J. Nucl. Mater. **145–147**, 241 (1987).
[86] H. Lin, R. D. Bengtson, and Ch. P. Ritz, Phys. Fluids B **1**, 2027 (1989).
[87] V. P. Budaev and R. S. Ivanov, in *Proceedings of the 12th European Conference on Controlled Fusion and Plasma Physics* (European Physical Society, Petit-Lancy, Switzerland, 1985), Vol. 1, p. 303.
[88] B. Zurro *et al.*, in *Plasma Physics and Controlled Nuclear Fusion Research 1988*, Nice (IAEA, Vienna, 1989), Vol. 1, p. 299.
[89] C. Hidalgo, M. A. Pedrosa, A. P. Navarro, and E. Escasibar, in *Proceedings of the 16th European Conference on Controlled Fusion and Plasma Physics* (European Physical Society, Petit-Lancy, Switzerland, 1989), Vol. 3, p. 927.
[90] P. Mantica *et al.*, in *Proceedings of the 16th European Conference on Controlled Fusion and Plasma Physics* (European Physical Society, Petit-Lancy, Switzerland, 1989), Vol. 3, p. 967.
[91] A. Rudyj *et al.*, in *Proceedings of the 16th European Conference on Controlled Fusion and Plasma Physics* (European Physical Society, Petit-Lancy, Switzerland, 1989), Vol. 1, p. 27.
[92] D. R. Thayer and P. H. Diamond, Phys. Fluids **30**, 3724 (1987).
[93] P. C. Stangeby and G. M. McCracken, submitted to Nucl. Fusion (1989).
[94] D. C. Robinson and M. G. Rusbridge, Plasma Phys. **11**, 73 (1969).
[95] K. Miyamoto, Nucl. Fusion **18**, 243 (1978).
[96] F. Sano *et al.*, Nucl. Fusion **26**, 473 (1986).
[97] L. Armi and P. Flament, J. Geophys. Res. **90**, 11779 (1985).
[98] J. Stockel *et al.*, in *Plasma Physics and Controlled Nuclear Fusion Research 1988*, Nice (IAEA, Vienna, 1989), Vol. 1, p. 359.
[99] M. Keilhacker *et al.*, Phys. Scr. **T2**, 443 (1982).
[100] F. Wagner and K. Lackner, in *Physics of Plasma-Wall Interactions in Controlled Fusion*, edited by D. E. Post and R. Behrisch (Plenum, New York, 1986), p. 731.
[101] L. Oren, L. Keller, F. Schwirzke, S. Talmadge, and R. J. Taylor, J. Nucl. Mater. **111–112**, 34 (1982).
[102] P. E. Phillips *et al.*, J. Nucl. Mater. **145–147**, 807 (1987).
[103] G. N. Fidel'man, R. S. Ivanov, and G. J. Stotsky, in *Proceedings of the 11th European Conference on Controlled Fusion and Plasma Physics* (European Physical Society, Petit-Lancy, Switzerland, 1983), Vol. 2, p. 409.
[104] G. N. Fidel'man, Sov. J. Plasma Phys. **11**, 376 (1985).
[105] C. S. Pitcher, D. H. J. Goodall, G. F. Matthews, G. M. McCracken, and P. C. Stangeby, in *Proceedings of the 14th European Conference on Controlled Fusion and Plamsa Physics* (European Physical Society, Petit-Lancy, Switzerland, 1987), Vol. 2, p. 736.
[106] J. J. Ellis, A. A. Howling, A. W. Morris, and D. C. Robinson, in *Plasma*

Physics and Controlled Nuclear Fusion Research 1984, London (IAEA, Vienna, 1985), Vol. 1, p. 363.
[107] M. Hedemann, Ph.D. thesis, California Institute of Technology, 1981.
[108] P. W. Terry and P. H. Diamond, Phys. Fluids **28**, 1419 (1985).
[109] L. Garcia, P. H. Diamond, B. A. Carreras, and J. D. Callen, Phys. Fluids **28**, 2147 (1985).
[110] T. S. Hahm, P. H. Diamond, P. W. Terry, L. Garcia, and B. A. Carreras, Phys. Fluids **30**, 1452 (1987).
[111] Y. J. Kim, Ph.D. thesis, The University of Texas at Austin, 1989.
[112] T. Chiueh, P. W. Terry, P. H. Diamond, and J. E. Sedlak, Phys. Fluids **29**, 231 (1986).
[113] R. E. Slusher and C. M. Surko, Phys. Rev. Lett. **40**, 400 (1978).
[114] C. M. Surko and R. E. Slusher, Phys. Fluids **23**, 2425 (1980).
[115] EQUIPE TFR, in *Plasma Physics and Controlled Nuclear Fusion Research 1976*, Berchtesgaden (IAEA, Vienna, 1977), Vol. 1, p. 35.
[116] EQUIPE TFR, in *Controlled Fusion and Plasma Physics*, Proceedings of the 8th European Conference, Prague, 1977 (European Physical Society, Petit-Lancy, Switzerland, 1977), Vol. 1, p. 2.
[117] TFR Group and A. Truc, Plasma Phys. Controlled Fusion **26**, 1045 (1984).
[118] EQUIPE TFR, Plasma Phys. **25**, 641 (1983).
[119] T. Crowley and E. Mazzucato, Nucl. Fusion **25**, 507 (1985).
[120] E. Mazzucato, Phys. Rev. Lett. **48**, 1828 (1982).
[121] A. J. H. Donne *et al.*, in *Proceedings of the 14th European Conference on Controlled Fusion and Plasma Physics* (European Physical Society, Petit-Lancy, Switzerland, 1987), Vol. 1, p. 245.
[122] G. Dodel and E. Holzhauer, in *Proceedings of the 15th European Conference on Controlled Fusion and Plasma Physics* (European Physical Society, Petit-Lancy, Switzerland, 1988), Vol. 1, p. 43.
[123] G. Dodel, E. Holzhauer, J. Massig. J. Gernhardt, ASDEX-, ICRH-, LH-, NI-, and Pellet Teams, in *Proceedings of the 14th European Conference on Controlled Fusion and Plasma Physics* (European Physical Society, Petit-Lancy, Switzerland, 1987), Vol. 1, p. 249.
[124] G. Dodel and E. Holzhauer, in *Proceedings of the 16th European Conference on Controlled Fusion and Plasma Physics* (European Physical Society, Petit-Lancy, Switzerland, 1989), Vol. 1, p. 163.
[125] J. Forster, Ph.D. thesis, Rensselaer Polytechnic Institute, 1988.
[126] P. M. Schoch, J. C. Forster, R. L. Hickok, and A. J. Wootton, in *Proceedings of the 14th European Conference on Controlled Fusion and Plasma Physics* (European Physical Society, Petit-Lancy, Switzerland, 1987), Vol. 1, p. 126.
[127] D. L. Brower, W. A. Peebles, N. C. Luhmann, Jr., and R. L. Savage, Phys. Rev. Lett. **54**, 689 (1985).
[128] R. L. Watterson, R. E. Slusher, and C. M. Surko, Phys. Fluids **28**, 2857 (1985).
[129] E. J. Doyle and D. E. Evans, Rev. Sci. Instrum. **59**, 1574 (1988).
[130] B. Lipshultz *et al.*, Nucl. Fusion **24**, 977 (1984).
[131] D. L. Brower, W. A. Peebles, and N. C. Luhmann, Jr., Phys. Rev. Lett. **55**, 2579 (1985).
[132] E. Mazzucato, Phys. Fluids **21**, 1063 (1978).
[133] R. E. Slusher *et al.*, Phys. Rev. Lett. **53**, 667 (1984).
[134] D. L. Brower *et al.*, in *Controlled Fusion and Plasma Physics*, Proceedings of the 15th European Conference, Dubrovnik (European Physical Society, Petit-Lancy, Switzerland, 1983), Vol. 1, p. 183.
[135] D. L. Brower *et al.*, Nucl. Fusion **29**, 1247 (1989).
[136] W. Horton, Phys. Fluids **19**, 711 (1976).
[137] P. Similon and P. H. Diamond, Phys. Fluids **27**, 916 (1984).
[138] G. S. Lee and P. H. Diamond, Phys. Fluids **29**, 3291 (1986).
[139] P. W. Terry, J. N. Leboeuf, P. H. Diamond, D. R. Thayer, J. E. Sedlak, and G. S. Lee, Phys. Fluids **31**, 2920 (1988).
[140] N. Mattor and P. H. Diamond, Phys. Fluids B **1**, 1980 (1989).
[141] A. J. Wootton *et al.*, Plasma Phys. Controlled Fusion **30**, 1479 (1988).
[142] W. M. Tang, Nucl. Fusion **18**, 1089 (1978).
[143] W. Horton, in *Basic Plasma Physics, II*, edited by A. A. Galeev and R. N. Sudan (North-Holland, Amsterdam, 1985), p. 383.
[144] E. Mazzucato, Phys. Rev. Lett. **36**, 792 (1976).
[145] P. Valanju (private communication, 1989).
[146] N. L. Vasin, V. A. Vershkov, and V. A. Zhuraviev, Sov. J. Plasma Phys. **10**, 645 (1984).
[147] P. C. Efthimion *et al.*, in *Plasma Physics and Controlled Nuclear Fusion Research 1988*, Nice (IAEA, Vienna, 1989), Vol. 1, p. 307.
[148] G. M. Batanov *et al.*, in *Proceedings of the 15th European Conference on Controlled Fusion and Plasma Physics* (European Physical Society, Petit-Lancy, Switzerland, 1988), Vol. 2, p. 455.
[149] M. Okabayashi and R. Freeman, Phys. Fluids **15**, 359 (1972).
[150] TFR Group and A. Truc, Nucl. Fusion **26**, 1303 (1986).
[151] D. Frigione and S. Goetsch, in *Proceedings of the 16th European Conference on Controlled Fusion and Plasma Physics* (European Physical Society, Petit-Lancy, Switzerland, 1989), Vol. 1, p. 143.
[152] TFR group and A. Truc, in *Turbulence and Anomalous Transport in Magnetized Plasmas*, Cargese Workshop 1986, edited by D. Gresillon and M. Dubois (Ecole Polytechnique, Palaiseau, France, 1986), p. 141.
[153] P. Schoch (private communication, 1989).
[154] F. Romanelli, W. M. Tang, and R. B. White, Nucl. Fusion **26**, 1515 (1986).
[155] R. R. Dominguez and R. E. Waltz, Nucl. Fusion **27**, 65 (1987).
[156] A. Rogister, G. Hasselberg, F. W. Waelbroeck, and J. Weiland, Nucl. Fusion **28**, 1053 (1988).
[157] TFR group and D. Gresillon, in *Turbulence and Anomalous Transport in Magnetized Plasmas*, Cargese Workshop 1986, edited by D. Gresillon and M. Dubois (Ecole Polytechnique, Palaiseau, France, 1986), p. 145.
[158] F. Gervais, D. Gresilon, P. Hennequin, A. Quemeneur, and A. Truc, in *Proceedings of the 16th European Conference on Controlled Fusion and Plasma Physics* (European Physical Society, Petit-Lancy, Switzerland, 1989), Vol. 2, p. 497.
[159] H. W. H. Van Andel, A. Boileau, and M. Von Hellermann, Plasma Phys. Controlled Fusion **29**, 49 (1987).
[160] A. Rogister *et al.*, Nucl Fusion **26**, 797 (1986).
[161] M. Jadoul and G. Waidmann, in *Proceedings of the 16th European Conference on Controlled Fusion and Plasma Physics* (European Physical Society, Petit-Lancy, Switzerland, 1989), Vol. 2, p. 529.
[162] D. L. Brower, W. A. Peebles, S. K. Kim, and N. C. Luhmann, Jr., in *Proceedings of the 14th European Conference on Controlled Fusion and Plasma Physics* (European Physical Society, Petit-Lancy, Switzerland, 1987), Vol. 3, p. 1314.
[163] A. Boileau, H. W. H. Van Andel, M. Von Hellermann, and A. Rogister, Nucl. Fusion **27**, 109 (1987).
[164] P. Schoch *et al.*, in *Proceedings of the 15th European Conference on Controlled Fusion and Plasma Physics* (European Physical Society, Petit-Lancy, Switzerland, 1988), Vol. 1, p. 191.
[165] C. S. Chang and F. L. Hinton, Phys. Fluids **29**, 3314 (1986).
[166] S. M. Wolfe and M. N. Greenwald, Nucl. Fusion **26**, 329 (1986).
[167] M. Greenwald *et al.*, Phys. Rev. Lett. **53**, 352 (1984).
[168] B. Coppi, M. N. Rosenbluth, and R. Z. Sagdeev, Phys. Fluids **10**, 582 (1967).
[169] B. B. Kadomtsev and O. P. Pogutse, in *Reviews of Plasma Physics*, edited by M. A. Leontovich (Consultants Bureau, New York, 1970), Vol. 5, p. 249.
[170] J. W. Connor, Nucl. Fusion **26**, 193 (1986).
[171] B. C. Hong and W. Horton, submitted to Nucl. Fusion (1989).
[172] D. C. Robinson and K. McGuire, Nucl. Fusion **19**, 115 (1979).
[173] J. D. Callen, J. P. Christiansen, and J. G. Cordey, Nucl. Fusion **27**, 1857 (1987).
[174] Z. Chang and J. D. Callen, submitted to Nucl. Fusion (1989).
[175] B. Kadomtsev, Sov. J. Plasma Phys. **1**, 389 (1975).
[176] D. J. Cambell *et al.*, Nucl. Fusion **26**, 1085 (1986).
[177] H. Soltswich, Rev. Sci. Instrum. **57**, 1939 (1986).
[178] W. P. West, D. M. Thomas, and J. deGrassie, Phys. Rev. Lett. **58**, 2758 (1987).
[179] H. Soltswich, W. Stodiek, J. Manickam, and J. Schluter, in *Plasma Physics and Controlled Nuclear Fusion Research 1986*, Kyoto (IAEA, Vienna, 1987), Vol. 1, p. 263.
[180] J. A. Wesson, Nucl. Fusion **18**, 87 (1978).
[181] J. A. Wesson, *Tokamaks* (Clarendon, Oxford, 1987).
[182] J. D. Callen *et al.*, in *Plasma Physics, and Controlled Fusion Research 1978*, Innsbruck (IAEA, Vienna, 1979), Vol. 1, p. 415.
[183] M. Z. Tokar, in *Proceedings of the 14th European Conference on Controlled Fusion and Plasma Physics* (European Physical Society, Petit-Lancy, Switzerland, 1987), Vol. 2, p. 687.
[184] S. M. McCool *et al.*, submitted to Nucl. Fusion (1989).
[185] L. I. Artemenkov *et al.*, Sov. J. Plasma Phys. **6**, 346 (1980).
[186] L. A. Artsimovich, Nucl. Fusion **12**, 215 (1972).
[187] J. Dunlap *et al.*, Phys. Rev. Lett. **48**, 538 (1982).
[188] F. A. Roy, W. A. Cooper, F. Yasseen, and A. Turnbull, Plasma Phys. Controlled Fusion **30**, 1597 (1988).
[189] R. D. Stambaugh *et al.*, in *Plasma Physics and Controlled Nuclear Fusion Research 1984*, London (IAEA, Vienna, 1985), Vol. 1, p. 217.
[190] K. McGuire *et al.*, Phys. Rev. Lett. **50**, 891 (1983).

[191] F. Wagner *et al.*, Phys. Rev. Lett. **49**, 1408 (1982).
[192] R. J. Fonck *et al.*, in *Proceedings of the 4th International Symposium on Heating in Toroidal Plasmas*, Rome, 1984 (ENEA, Rome, 1984), Vol. 1, p. 37.
[193] R. D. Stambaugh *et al.*, Plasma Phys. Controlled Fusion **30**, 1585 (1988).
[194] J. Manickam and the TFTR Group, in *Plasma Physics and Controlled Nuclear Fusion Research 1988*, Nice (IAEA, Vienna, 1989), Vol. 1, p. 395.
[195] E. J. Strait *et al.*, in *Plasma Physics and Controlled Nuclear Fusion Research 1988*, Nice (IAEA, Vienna, 1989), Vol. 1, p. 83.
[196] M. Okabayashi *et al.*, in *Plasma Physics and Controlled Nuclear Fusion Research 1988*, Nice (IAEA, Vienna, 1989), Vol. 1, p. 97.
[197] N. V. Ivanov, I. A. Kovan, and I. B. Semonov, Sov. J. Plasma Phys. **3**, 526 (1977).
[198] J. W. Connor, in *Turbulence and Anomalous Transport in Magnetized Plasmas*, Cargese Workshop 1986, edited by D. Gresillon and M. Dubois (Ecole Polytechnique, Palaiseau, France, 1986), p. 53.
[199] K. W. Gentle, Y. J. Kim, Ch. P. Ritz, and T. L. Rhodes, in *Proceedings of the 14th European Conference on Controlled Fusion and Plasma Physics* (European Physical Society, Petit-Lancy, Switzerland, 1987), Vol. 1, p. 81.
[200] M. Malacarne and P. A. Duperrex, Nucl. Fusion **27**, 2113 (1987).
[201] Y. J. Kim, K. W. Gentle, C. P. Ritz, T. L. Rhodes, and R. D. Bengtson, Nucl. Fusion **29**, 99 (1989).
[202] R. E. Waltz, Phys. Fluids **28**, 577 (1985).
[203] F. Haas and A. Thyagaraja, in *Proceedings of the 15th European Conference on Controlled Fusion and Plasma Physics* (European Physical Society, Petit-Lancy, Switzerland, 1988), Vol. 1, p. 270.
[204] C. H. Hollenstein *et al.*, in *Turbulence and Anomalous Transport in Magnetized Plasmas*, Cargese Workshop 1986, edited by D. Gresillon and M. Dubois (Ecole Polytechnique, Palaiseau, France, 1986), p. 181.
[205] P. Duperrex *et al.*, Phys. Lett. **106A**, 133 (1984).
[206] B. Carreras *et al.*, Phys. Rev. Lett. **50**, 503 (1983).
[207] M. Murakami *et al.*, in *Plasma Physics and Controlled Nuclear Fusion Research 1982*, Baltimore (IAEA, Vienna, 1983), Vol. 1, p. 57.
[208] N. Ohyabu *et al.*, Phys. Rev. Lett. **58**, 120 (1987).
[209] D. C. Robinson *et al.*, in *Plasma Physics and Controlled Nuclear Fusion Research 1984*, London (IAEA, Vienna, 1985), Vol. 1, p. 205.
[210] F. Crisanti, M. Marinucci, and C. Nardone, in *Proceedings of the 16th European Conference on Controlled Fusion and Plasma Physics* (European Physical Society, Petit-Lancy, Switzerland, 1989), Vol. 1, p. 139.
[211] S. M. McCool *et al.*, Nucl. Fusion **29**, 547 (1989).
[212] K. Molvig, J. Rice, and M. Tekula, Phys. Rev. Lett. **41**, 1240 (1978).
[213] V. I. Bugarya *et al.*, Nucl. Fusion **25**, 1707 (1985).
[214] S. M. Kaye, Phys. Fluids **28**, 2827 (1985).
[215] V. V. Arsenin and V. A. Chuyanov, Sov. Phys. Usp. **20**, 736 (1977).
[216] R. Scarmozzino, A. K. Sen, and G. A. Navratil, Phys. Rev. Lett. **57**, 1729 (1986).
[217] A. D. Cheetham *et al.*, in *Plasma Physics and Controlled Nuclear Fusion Research 1988* Nice (IAEA, Vienna, 1989), Vol. 1, p. 483.